ABSTRACT

Performance of the NSSL Hail Detection Algorithm for Multicell Storms over the Coastal Southern Plains. (August 1999)

Capt. Kyle G. Bellue, USAF

Chair of Advisory Committee: Dr. Michael I. Biggerstaff, Texas A&M University

A study of the National Severe Storm Laboratory's (NSSL's) Hail Detection Algorithm (HDA) has been performed for over 20 different multicell storm systems that occurred over the coastal region of the southern Great Plains. Since the HDA was developed using a data set mostly from the Central Plains where many of the thunderstorms are supercellular, this study addresses the regional and storm morphological influences on the algorithm performance.

To enable use of ground validation from spotter networks, only the severe hail category was studied. While the NSSL HDA performed quite well in most instances, there was a tendency for the algorithm to over-warn for severe hail. Certain adjustable parameters within the HDA were tested for accuracy and optimized for the League City National Weather Service Office in Houston, Texas. These parameters include the Warning Threshold Selection Model (WTSM), the optimum population density threshold, and the Probability of Severe Hail (POSH) function.

PERFORMANCE OF THE NSSL HAIL DETECTION ALGORITHM FOR MULTICELL STORMS OVER THE COASTAL SOUTHERN PLAINS

A Thesis

by

KYLE GORDON BELLUE

Submitted to the Office of Graduate Studies of
Texas A&M University
in partial fulfillment of the requirements for the degree of

MASTER OF SCIENCE

August 1999

Major Subject: Meteorology

REPORT DOCUMENTATION PAGE

Form Approved
OMB No. 0704-0188

1. AGENCY USE ONLY *(Leave blank)*	2. REPORT DATE	3. REPORT TYPE AND DATES COVERED
	27.Jul.99	THESIS

4. TITLE AND SUBTITLE
PERFORMANCE OF THE NSSL HAIL DETECTION ALGORITHM FOR MULTICELL STORMS OVER TE COASTAL SOUTHERN PLAINS

5. FUNDING NUMBERS

6. AUTHOR(S)
CAPT BELLUE KYLE G

7. PERFORMING ORGANIZATION NAME(S) AND ADDRESS(ES)
TEXAS A&M UNIVERSITY

8. PERFORMING ORGANIZATION REPORT NUMBER

9. SPONSORING/MONITORING AGENCY NAME(S) AND ADDRESS(ES)
THE DEPARTMENT OF THE AIR FORCE
AFIT/CIA, BLDG 125
2950 P STREET
WPAFB OH 45433

10. SPONSORING/MONITORING AGENCY REPORT NUMBER
FY99-160

11. SUPPLEMENTARY NOTES

12a. DISTRIBUTION AVAILABILITY STATEMENT
Unlimited distribution
In Accordance With AFI 35-205/AFIT Sup 1

12b. DISTRIBUTION CODE

13. ABSTRACT *(Maximum 200 words)*

14. SUBJECT TERMS

15. NUMBER OF PAGES
66

16. PRICE CODE

17. SECURITY CLASSIFICATION OF REPORT	18. SECURITY CLASSIFICATION OF THIS PAGE	19. SECURITY CLASSIFICATION OF ABSTRACT	20. LIMITATION OF ABSTRACT

PERFORMANCE OF THE NSSL HAIL DETECTION ALGORITHM FOR MULTICELL STORMS OVER THE COASTAL SOUTHERN PLAINS

A Thesis

by

KYLE GORDON BELLUE

Submitted to Texas A&M University
in partial fulfillment of the requirements
for the degree of

MASTER OF SCIENCE

Approved as to style and content by:

Michael I. Biggerstaff
(Chair of Committee)

Richard E. Orville
(Member)

Thomas M. Over
(Member)

Gerald R. North
(Head of Department)

August 1999

Major Subject: Meteorology

DEDICATION

I would like to dedicate this thesis to my wonderful and loving wife, Luz Gomes Oliviera Martins Bellue. She has stood by my side through these difficult times and has selflessly endured my many days and nights away from home in order for me to achieve my goal. I am also grateful to my parents, Dan and Judy Bellue, for their constant love and encouragement.

ACKNOWLEDGEMENTS

I owe my deepest thanks to Dr. Michael I. Biggerstaff for keeping his promise and driving me to finish on time. Without his leadership and knowledge, I would have not been able to complete the project when I did. To my other committee members, thanks for serving on my committee and for your advice and suggestions regarding this thesis. I am also very grateful to Arthur Witt at the National Severe Storms Laboratory who patiently took the time to help me get a firm grasp on how their algorithms operated. Thanks must go out to Gordon Carrie, who got me out of some major computer programming jams....more than once! I would also like to thank Beth Karl who taught me how to use the radar software. Thanks also to my fellow AFIT students who pushed me to excel in my classwork. A special thanks to all those who participated with me in relieving graduate school stress by playing "hacky-sack" outside the O&M building. Those breaks were well worth it.

This work was supported by a grant from the Texas Higher Education Coordinating Board's Advanced Research Program (010366-151) and by a grant from NASA (NAG 5-4776).

Finally, I would like to thank the Air Force Institute of Technology at Wright Patterson Air Force Base, Ohio for selecting me into this program so that I could further my knowledge about meteorology.

TABLE OF CONTENTS

	Page
ABSTRACT	iii
DEDICATION	iv
ACKNOWLEDGEMENTS	v
TABLE OF CONTENTS	vi
LIST OF FIGURES	viii
LIST OF TABLES	x
CHAPTER	
I INTRODUCTION AND PREVIOUS STUDIES	1
a. Introduction	1
b. Previous studies	4
II NSSL HAIL DETECTION ALGORITHM DESIGN	6
a. POH	9
b. POSH	9
III DATA AND METHOD OF ANALYSIS	14
a. Data	14
b. Method of analysis	16
IV RESULTS	27
a. NSSL hail study results	27
b. League City hail performance results	30
VI CONCLUSIONS	54
REFERENCES	57
APPENDIX A	60
APPENDIX B	63

Page

APPENDIX C 64

APPENDIX D 65

VITA 66

LIST OF FIGURES

		Page
Figure 1:	The NWS League City county warning area	2
Figure 2:	This image represents the joining of three adjacent storm segments into a 2D-storm component	7
Figure 3:	This figure shows the WATADS radar display for Walker County on 21 January 1998	8
Figure 4:	Graph showing relationship between POH and the height of the melting level (H_0) and the height of the 45 dBZ reflectivity core	10
Figure 5:	Reliability diagram for the probability of severe hail for 10 days of radar data from Oklahoma and Florida	20
Figure 6:	This figure shows the optimum warning threshold (black line) as a function of the melting layer from the initial HDA tests made by NSSL	22
Figure 7:	Same as Figure 5, but data comes from regional NSSL study performed over 31 storm days and 7 radar locations	29
Figure 8a:	WTSM plot for all continental-forced hail days	34
Figure 8b:	Same as Fig. 8a, but for all seabreeze-forced hail days	34
Figure 8c:	Same as Fig. 8a, but for all Spring/Summer hail days	35
Figure 8d:	Same as Fig. 8a, but for all Fall/Winter hail days	35
Figure 8e:	Same as Fig. 8a, but for all continental-Spring/Summer hail days	36
Figure 8f:	Same as Fig. 8a, but for all seabreeze-Spring/Summer hail days	36
Figure 8g:	Same as Fig. 8a, but for all continental-Fall/Winter hail days	37
Figure 8h:	Same as Fig. 8a, but for all 18 hail days	37
Figure 9:	This is the reliability graph for the League City county warning area using only the default algorithm values	39

Page

Figure 10: This is a graph showing the cumulative frequency distributions of both the observed and forecasted POSH values 39

Figure 11: This figure shows the statistical scoring values plotted against certain population density thresholds 40

Figure 12: This figure shows the cumulative frequency distribution of the observed hail occurrences based on population density threshold values versus the population density distributions over the League City county warning area 40

Figure 13: Same as Figure 9, except this figure includes the results from running the hail algorithm using the optimized WTSM values for the League City warning area 44

Figure 14: Same as Figure 10, except this figure shows the statistical results from running the hail algorithm using an optimized WTSM line 44

Figure 15: Same as Figure 13, except this figure includes the results from altering the POSH probability equation 46

Figure 16: Same as Figure 10, except this figure shows the statistical results from running the hail algorithm after altering the POSH probability equation 47

Figure 17: This figure shows the change in the reliability of a subset of data used to test the radar sensitivity to a 2 dBZ reflectivity adjustment 52

Figure 18: This figure shows the frequency of forecasted POSH values when the algorithm was run using the 2 dBZ adjustment 53

LIST OF TABLES

		Page
Table 1:	Complete listing of hail reports used for this study	15
Table 2:	The partial hail-truth file for hail reported on 03 November 1995	19
Table 3:	2X2 contingency table of forecast versus observed states, used to determine statistical scores for Y (yes) / N (no) predictions of an event	19
Table 4:	Performance results from the hail algorithm for 09 September 1997 using the 20-minute time window	24
Table 5:	This table shows the regions used for the NSSL hail algorithm study	28
Table 6:	Regional performance results for the NSSL study	28
Table 7:	Data analyzed from the League City radar	31
Table 8:	Same as Table 7, except data is divided by time of occurrence, namely either Spring/Summer or Fall/Winter	32
Table 9:	Same as Table 7, except this table shows the statistical results from running the hail algorithm using an optimized WTSM line	42
Table 10:	Same as Table 8, except this table shows the statistical results from running the hail algorithm using an optimized WTSM line	43
Table 11:	Same as Table 9, except this table shows the statistical results from running the hail algorithm using an optimized POSH equation	48
Table 12:	Same as Table 10, except this table shows the statistical results from running the hail algorithm using an optimized POSH equation	49
Table 13:	This table shows the statistical performance of the HDA when 2 dBZ were added to all reflectivity values	51

CHAPTER I

INTRODUCTION AND PREVIOUS STUDIES

a. Introduction

The accuracy and timeliness of severe weather warnings depend on both the availability of observations from weather radars used by the National Weather Service (NWS), and a thorough understanding of the different types of storm structures and environments that can produce severe weather. To help meet this challenge, the NWS has recently deployed a Doppler weather radar network across Texas and much of the nation (Klazura and Imy 1993), where each site is responsible for severe weather warnings over a 125 nautical mile range. In an attempt to automate the detection and interpretation of severe weather signatures observed by Doppler radar, the NWS relies on computer-based algorithm software, some of which has been developed by the National Severe Storms Laboratory (NSSL) in Norman, Oklahoma. This software is used in conjunction with the WSR-88D (Weather Surveillance Radar – 1988 Doppler) to examine the incoming data for well-known, classic storm structures and to determine whether or not the storm structure is severe. One such algorithm analyzes convective cell structure to determine the likelihood of severe hail (greater than 0.75 inches in diameter) within that cell.

Thunderstorms that produce severe hail have proven to be very costly to both densely populated areas and to agricultural interests in rural areas. The NWS office in League City, Texas, located just south of Houston, is responsible for providing weather warnings to a wide range of counties including rural areas such as Houston, Trinity, Chambers, Madison, Brazoria and Brazos counties to densely populated counties such as Harris and Galveston counties (Figure 1).

This thesis follows the style of the *Journal of Applied Meteorology.*

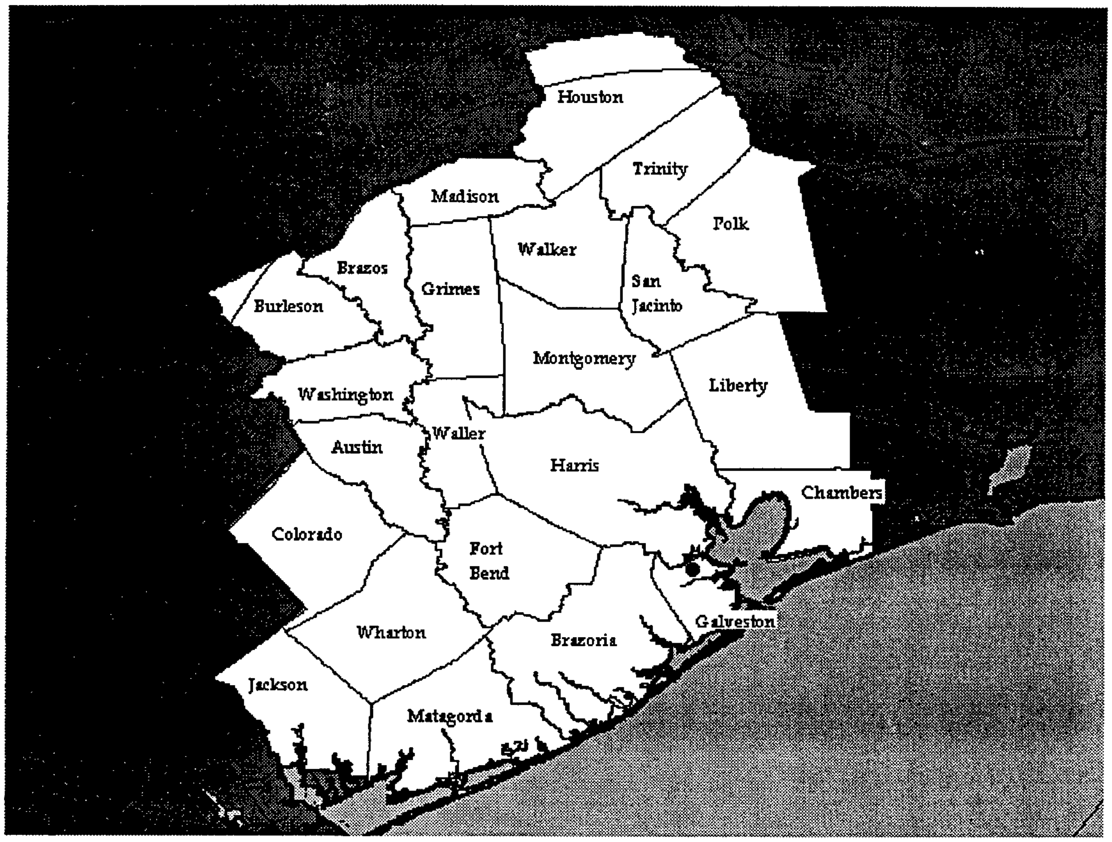

Figure 1. The NWS League City county warning area. The black dot indicates the NWS office at League City, Texas. The black circle represents the 200 kilometer range of the WSR-88D radar located at the NWS office.

In this warning region alone there was an estimated $105K worth of hail damage in 1995 (NOAA 1995), $5.5M worth of hail damage in 1996 (NOAA 1996), and close to $600K in 1997 (NOAA 1997). The ability to detect, or predict, severe hail within thunderstorms might aid in minimizing the losses due to this damaging weather phenomenon.

The conceptual models and databases used to develop the hail detection algorithm (HDA) were based mostly on observations in the Central Great Plains of the United States (Witt et al. 1998). It is unclear whether these data sets are sufficient for severe weather events that occur along the Texas Gulf coast. In this area, the weather regime is semitropical and is mostly dominated by warm moist air that flows northward from the Gulf of Mexico. Weather events initiated in this area have a more complex convective nature where the environment is more moist and the wind shear is weak. This is in direct contrast to the Central Great Plains, where the air above the boundary layer is drier and the wind shear is more pronounced.

Because regional variability in storm structure was known to exist before radar deployment, NSSL has developed the WSR-88D Algorithm Testing and Display System (WATADS). This system allows individual NWS offices to perform local evaluations of the algorithms to determine the optimum threshold values for their particular warning area. This is made possible because many of the automated computer algorithms within WATADS contain site adaptable parameters that can be adjusted to improve the detection of severe weather in regions where the Central Great Plains conceptual models do not apply (Crum et al. 1993). However, studies to provide guidance to the local NWS offices concerning parameter adjustments have been limited by lack of research access to real-time Doppler data, and the need for a critical evaluation of the modified algorithm's performance.

Currently, there have been no studies directed to developing a suitable set of adaptable parameters for the Texas Gulf coast. We address this concern here by performing an analysis of Texas Gulf coast storms to determine the optimal threshold values used in the HDA. By testing this algorithm in a natural environment that is different from where it was developed, it will be possible to provide more useful

guidance to the NWS offices in the State of Texas and the remainder of the Gulf coast region.

The focus and goal of this study will be two-fold. The first goal will be to see how the hail algorithm performs in the League City NWS county warning area using the WATADS software along with recently collected Level II radar and local environmental data. The second goal will be to take the information above, and try to improve the hail detection and warnings over this area by tuning the hail algorithm using systematic site-adaptable parameter adjustments.

b. Previous studies

The original WSR-88D Hail Algorithm was developed by Petrocchi (1982). The design was based on identification of the structural characteristics of typical severe hailstorms found in the Southern Plains (Lemon 1978). Lemon examined the entire three-dimensional reflectivity structure in identifying severe hailstorms. Using hailstorms case studies, he showed that the height of a given reflectivity value was more correlated with severe hailstorms than peak reflectivity values for a particular storm. He also showed that the position of the highest echo top relative to the low-level reflectivity core was strongly correlated with whether or not the storm will produce hail. Another major influence in hailstorm development was the extent of the Weak Echo Region of the storm, or the amount of overhang of the mid-level reflectivity echo. From these findings, several hail indicators were determined to be the most useful in representing the storm structure and the conditions necessary for hailstorm development (Smart and Alberty 1985). Appendix A gives a detailed description of these findings.

Early testing of this algorithm in the Central Plains showed good performance (Petrocchi 1982; Smart and Alberty 1985). However, subsequent testing by Winston (1988) over the Colorado High Plains showed relatively poor performance by the hail algorithm due, in large part, to the different weather regime in which the algorithm was tested. The algorithm's ability to distinguish hailstorms from non-hailstorms, or severe hailstorms from non-severe hailstorms, was not adequate.

Irrespective of its apparent lack of performance in other weather regimes, the utility of the hail algorithm was not of much use to NWS forecasters due to the nature of its output. Petrocchi's algorithm was only optimized to detect hail of size 1.25 inches or greater. Since NWS forecasters were required to provide warnings for severe size hail being ≥ 0.75 inches, they needed a modified algorithm optimized for this size and not the hail size as proposed by Petrocchi's algorithm.

This has led to the design and development of a new Hail Detection Algorithm (HDA) for the WSR-88D (Witt 1993). Given the uncertainties involved in characterizing hailstorms, empirical probability functions are now used. Also, in place of the previous labels, the new algorithm produces, for each detected storm cell, the following information: probability of hail of any size (POH), probability of severe hail (POSH), and maximum expected hail size (MEHS). All acronyms used during this study will be listed in Appendix B.

CHAPTER II

NSSL HAIL DETECTION ALGORITHM DESIGN

One of the latest algorithms to be placed into WATADS is the Hail Detection Algorithm. As mentioned above, the purpose of the NSSL HDA is to provide reliable estimates of the probability of hail, probability of severe hail, and the maximum expected hail size for each storm cell identified by the system. The HDA is composed of two sub-algorithms: the Hail Core Aloft Algorithm (HCAA) (Witt 1990; 1993) and the Upper-Level Divergence Algorithm (ULDA). However, since this study will only be examining an algorithm contained in the HCAA, the ULDA will not be discussed.

The HCAA currently produces all of the HDA output. The HCAA estimates the POH, the POSH (hail with diameter ≥ 0.75 in), and the MESH for each detected storm cell (Witt et al. 1998). This algorithm runs in conjunction with the Storm Cell Identification and Tracking (SCIT) algorithm developed at NSSL to locate and track the center of a storm cell. This algorithm process consists of basically four main steps.

The first step begins with the algorithm searching along the radials for data segments that contain reflectivities greater than a specified threshold. Each part of the ray of radar data that exceeds the threshold is referred to as a storm segment. Figure 2 shows separate storm segments with different threshold values along three adjacent radar rays. The second step involves combining the azimuthally adjacent segments into 2D-storm components, also shown in Figure 2. The algorithm then compiles the newly computed 2D information throughout all the volume scans and turns all of its vertically adjacent 2D components into "3D-storms". The storm cell in Figure A1 illustrates this process.

Finally, the SCIT algorithm produces output on the storm's structural characteristics and displays it on the WATADS radar reflectivity display. An illustration of the WATADS display is given on Figure 3. This data comes from 21 January 1998 and shows an example of the identification of storm centers by the SCIT

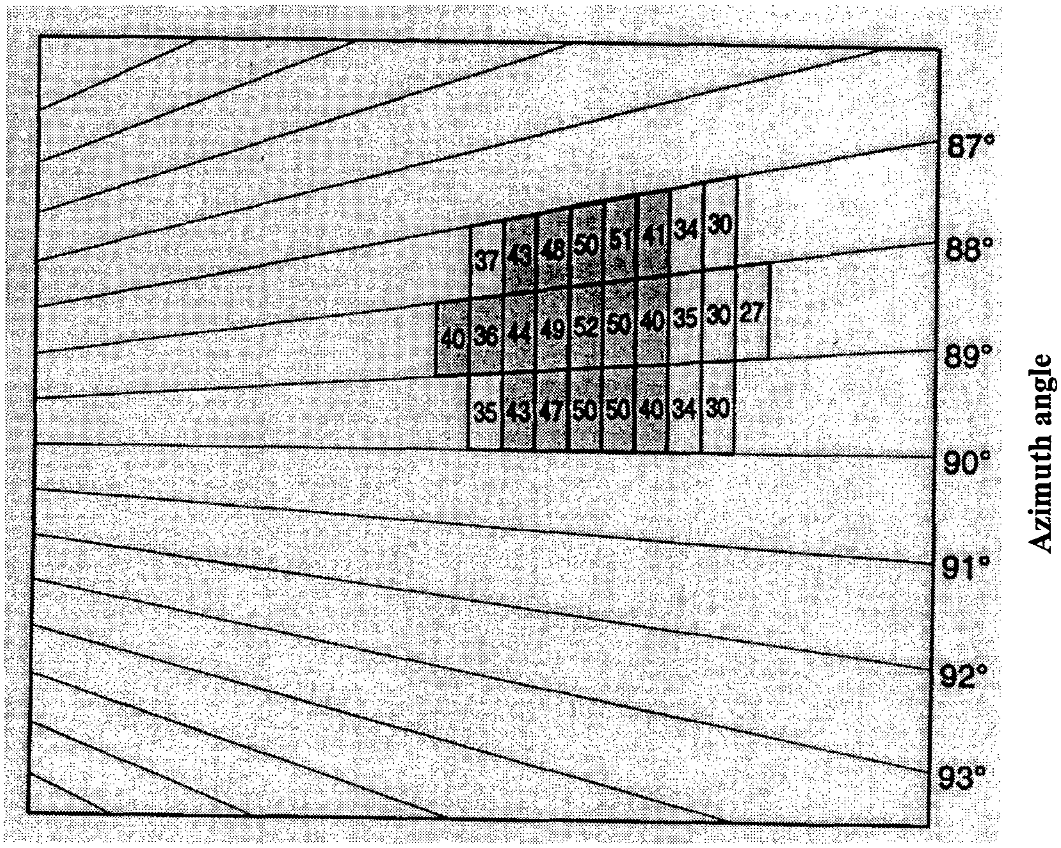

Figure 2. This image represents the joining of three adjacent storm segments into a 2D-storm component. The shading denotes a 40 dBz threshold. The graduated lines represent azimuthal radar beams at a fixed elevation angle. Adapted from Johnson et al. (1998).

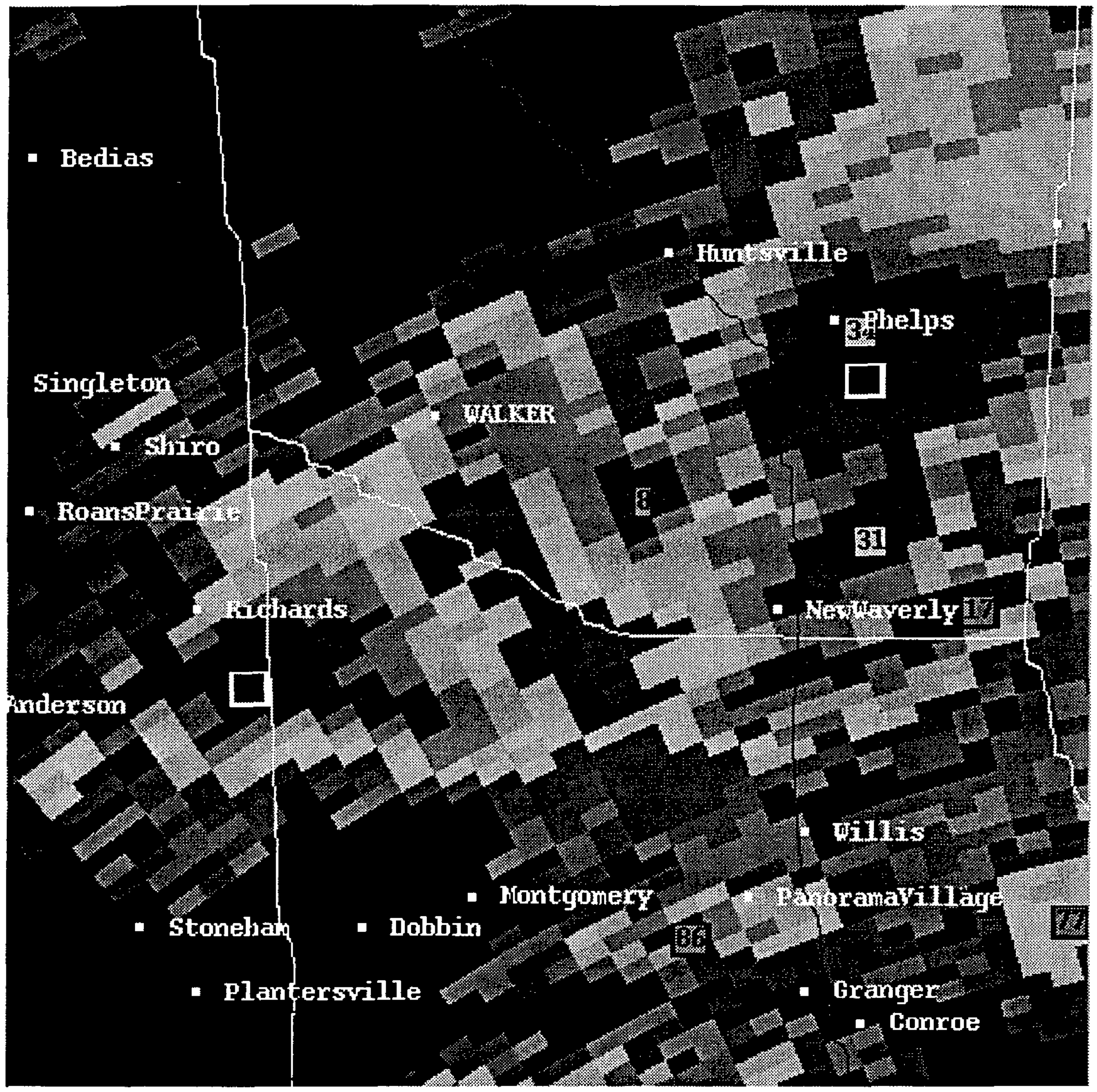

Figure 3. This figure shows the WATADS radar display for Walker County on 21 January 1998. The boxed values are the storm center values that the SCIT algorithm assigns to each storm cell. The dark-shaded boxes depict cells with POSH values > 50% (ex. #47). The light-shaded boxes depict cells with POSH values between 20% and 40% (ex. #31). The medium-shaded boxes depict cell with POSH values < 20% (ex. #8).

algorithm. The following paragraphs explain how the POH and POSH algorithms work, and elucidate all the parameters defined within them.

a. POH

To determine the POH of any size in a particular storm cell, the HDA employs an adaptation of a Waldvogel et al. (1979) relation between the height (km) of the 45 dBZ echo (H_{45}) and the height (km) of the freezing level (H_0) in determining the probability of hail reaching the ground. This is illustrated in Figure 4, which shows the relationship between POH and the difference between H_{45} and H_0. The greater the distance between the height of the 45 dBZ echo top and the height of the freezing level, the greater the POH. Since the algorithm's output has been converted to probabilities, Figure 4 shows percentages in increments of 10%. However, the values from this relation were derived using only hail storm data from a High Plains environment, so caution should be used when applying this to other environments.

b. POSH

The POSH parameter determines the probability of severe hail (diameter $\geq$ 0.75 inch). This probability is obtained with the following equation:

$$POSH = 29\ln\frac{SHI}{WT} + 50 \qquad (1)$$

where SHI is the Severe Hail Index and WT is the Warning Threshold function.

SHI was developed as the primary predictor for severe size hail. It uses an approach similar to the vertical integration of liquid (VIL), estimated from a reflectivity-liquid relationship, with a few improvements. The first improvement involves moving from a grid-based algorithm to a storm cell-based algorithm, using output from the SCIT algorithm discussed earlier. The advantage of a storm cell-based

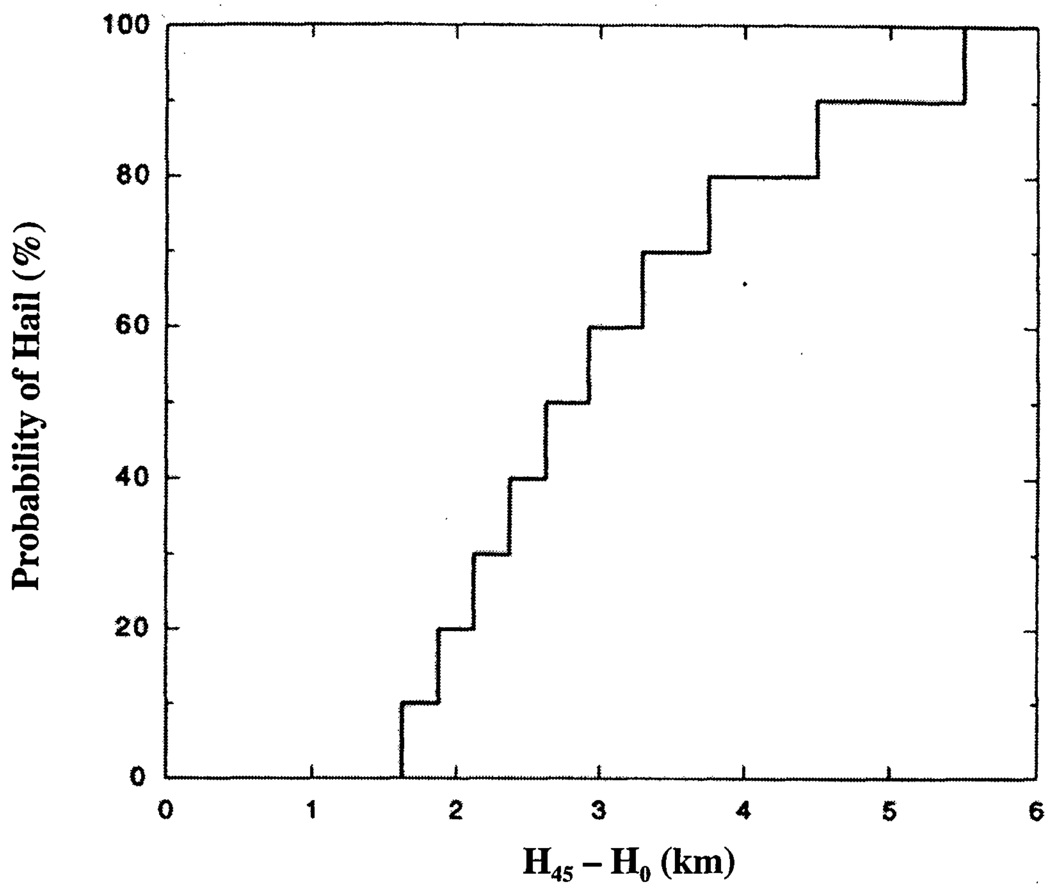

Figure 4. Graph showing relationship between POH and the height of the freezing level (H_0) and the height of the 45 dBZ reflectivity core. Derived from Waldvogel et al. (1979).

system is the problem associated with having a hail core cross a grid boundary, which occurs frequently, is eliminated. However, one disadvantage to this method is that if an error occurs in the cell identification process, this may cause an error in the HDA output.

The second improvement involves using a reflectivity-to-hail relation, based on Waldvogel et al. (1978a,b). Waldvogel derived a relationship between the radar reflectivity factor (Z) and the flux of kinetic energy ($\dot{E}$) by analyzing hail size distributions measured with hail spectrometers. This reflectivity-to-hail relation is similar in principle to the reflectivity-to-rainrate (Z-R) relation, used widely to estimate rainfall amounts, which analyzes variations of (Z-R) with raindrop disdrometers to represent an ideal raingage-radar combination (Waldvogel et al. 1978a). Here, Waldvogel discovered the hail spectrometer represented an ideal hailpad-radar combination. He also discovered that the variations in the Z-$\dot{E}$ relationship throughout a wide variety of storms tested were very small. Waldvogel developed a semi-empirical formula that could be computed by assuming Rayleigh scattering and an exponential size distribution for the hailstone spectra (Waldvogel et al. 1978a,b; Federer et al. 1986). Witt et al. (1998) modified the Hailfall Kinetic Energy equation by adding a weighting function such that:

$$\dot{E} = 5.0 \times 10^{-6} \times 10^{0.084Z} W(Z) \tag{2}$$

where $\dot{E}$ has units of J m^{-2} s^{-1}. Z is taken to be the logarithmic value of the radar reflectivity factor (measured in dBZ – explained in Appendix C) and W(Z) is the weighting function defined as:

$$W(Z) = \begin{cases} 0 & \text{for } Z \leq Z_L \\ \dfrac{Z - Z_L}{Z_U - Z_L} & \text{for } Z_L < Z < Z_U \\ 1 & \text{for } Z \geq Z_U \end{cases} \tag{3}$$

W(Z) is used to define a transition zone between rain and hail reflectivities. Z_U and Z_L are reflectivity upper and lower boundaries and are set by default as Z_U = 50 dBZ and Z_L = 40 dBZ. This Z-$\dot{E}$ relationship uses only the higher reflectivities typically associated with hail and filters out most of the lower reflectivities that are typically associated with liquid water.

The last improvement within the SHI involves the temperature range where hail is most likely to form. Because hail growth will only occur at temperatures < 0°C, and severe hail growth will only occur at temperatures < -20°C or colder (English 1973; Browning 1977; Nelson 1983; Miller et al. 1988), a unitless, temperature-weighted, vertically integrated function $W_T(H)$ is used within the SHI function. It is defined as:

$$W_T(H) = \begin{cases} 0 & \text{for } H \leq H_0 \\ \dfrac{H - H_0}{H_{m20} - H_0} & \text{for } H_0 < H < H_{m20} \\ 1 & \text{for } H \geq H_{m20} \end{cases} \tag{4}$$

Where H is the height above radar level (ARL), H_0 is the height (ARL) of the environmental melting level, and H_{m20} is the height (ARL) of the -20°C environmental temperature. All heights are in kilometers. This function weighs the temperatures below -20°C the strongest, gives temperatures between 0°C and -20°C a small factor in the equation, but completely negates any values warmer than 0°C. Both H_0 and H_{m20} can be determined from a nearby upper-air sounding.

Finally, using all of the above parameters we can obtain what is known as the Severe Hail Index, which has units of J m^{-1} s^{-1}.

$$SHI = 0.1 \int_{H_0}^{H_T} W_T(H)\dot{E}\,dH \tag{5}$$

where H_T is the height (in km) of the highest echo of the storm cell. In the HDA, SHI is calculated using information from the 2D-storm components for the cell being analyzed, with at least two components required for calculation. $\dot{E}$ is calculated using the maximum reflectivity value for each 2D-storm component. This value is then applied throughout the entire vertical depth of the 2D-storm component, or the entire "3D-storm".

From the Witt et al. study (1998), the SHI underwent developmental testing at NSSL, where they used data from 115 storm reports that included severe-size hail. From these reports, it was discovered that the optimum value of WT was highly correlated to the melting level of that day. From these results, a simple Warning Threshold Selection Model (WTSM) was created, and is defined as:

$$WT = 57.5H_0 - 121 \tag{6}$$

where WT has units in J $m^{-1}s^{-1}$ and H_0 has units in kilometers.

Both of these parameters proved fairly successful in testing done by NSSL, with over Critical Success Index (CSI) values of greater than 40% (Witt et al. 1998). The next and final step was to create an overall probability function that incorporated the two parameters. Since the data set was fairly small, a simple probability function was used.

This has led to the POSH equation (1). The POSH parameter is measured in percentiles that are rounded of to the nearest 10%, in order to avoid conveying an unrealistic degree of precision. POSH values < 0 are set to 0, while POSH values > 100 are set to 100. Note that the probability of severe hail is 50% when the value of the severe hail index is equal to that of the warning threshold.

CHAPTER III

DATA AND METHOD OF ANALYSIS

a. Data

The convective events used for this study occurred within the League City forecasting area of responsibility. The hailstorms chosen for this data set occurred both between the years 1994 and 1997, and mostly during the months of March through August. Based on *Storm Data* reports from NOAA, these months were the optimum times for severe hail to form over this warning area. The data set included level II radar data archived from the WSR-88D Doppler radar from the NWS office in League City, Texas. Environmental data were provided by upper-air soundings from Corpus Christi, Texas and Lake Charles, Louisiana; and hail verification reports were provided by *Storm Data.*

Level II radar data were the main data source for this study. The hail days were carefully chosen in conjunction with the storm data to find hail days around the Houston area with the maximum amount of hail verification. To examine the thermodynamics of the environment, soundings were obtained from the National Climatic Data Center and were then ingested into WATADS.

There were 120 total hail reports used for this study. They can be found on Table 1. Since this study will be examining the effects of different storm types on the hail algorithm, the data were divided between convective events forced by seabreeze fronts and those forced by continental fronts or troughs. Only 15 of the reports were associated with seabreeze fronts. Two-thirds of the events took place during the spring-summer seasons (March – August). The remainder of the reports was associated with frontally forced deep convection during the winter season.

Storm data that was located within the radar's cone of silence, less than a 30 kilometer radius, or at ranges greater than 200 kilometers were not analyzed. This exclusion is due to the radar's inability to give meaningful data at these ranges.

Table 1. Complete listing of hail reports used for this study. The data is broken down into hail reports from convection due to seabreeze fronts and convection due to cold fronts or troughs advecting into the warning area from the north/northwest. From radar archives at the NWS office in League City, Texas.

Date	**SEABREEZE DATA** Description	Number of Hail Reports
02 Jun 96	Outflow Boundary	3
03 Jun 96	Outflow Boundary	2
04 Jun 96	Outflow Boundary	7
21 May 97	Outflow Boundary	1
02 Sep 97	Outflow Boundary	2
	Total Seabreeze:	15

Date	**CONTINENTAL DATA** Description	Number of Hail Report
05 Apr 94	Cold Front / Severe Thunderstorms / Hail	8
15 Apr 94	Cold front	10
02 May 94	Bow Echo	11
11 May 95	Supercells / Hail	10
03 Nov 95	Cold Front / Heavy Thunderstorms / Hail / Wind	8
05 Apr 96	Severe Thunderstorms / Flooding	9
25 Apr 97	Trof / Thunderstorms / Small Hail	5
27 Apr 97	Trof / Thunderstorms / Small Hail	6
28 May 97	Thunderstorms / Hail / Heavy Rain	2
09 Sep 97	Cold Front / Hail	6
21 Jan 98	Cold Front / Hail / Flooding	8
22 Jan 98	Cold Front / Hail / Flooding	15
11 Apr 97	Trof / Thunderstorms	7
	Total Continental:	105
	TOTAL OF ALL HAIL REPORTS:	**120**

b. Method of analysis

1) SELECTING HAIL DAYS

Eighteen hail days were chosen from the archived level II radar data. There were no "non-hail days" chosen as part of this study. The addition of non-hail days into the data set would introduce more false alarms into the scoring, thereby indicating where the algorithm might be over-forecasting. While this is a valuable objective of this study, it can be accomplished without the inclusion of non-hail days based on two data-spacing factors: location and time.

The first factor deals with the location of the hail event. There are cases within this data set where two different weather events are affecting different parts of the warning area. For instance, radar data from one hail day includes hail verification from a storm event in the extreme northern counties. During the same period, storm cells develop in the extreme southern counties, yet are not verified by *Storm Data* as being hail-producing storms. However, the algorithm scoring from the southern county storms are included as part of the same hail verification in the north. These cases illustrate hail days coupled with non-hail occurrences, and can be included in the scoring to increase the false alarm rate, thereby providing more realistic results.

The second factor deals with time lapses between hail events. Included in the data set are days where the lapses between hail verification times exceed four hours. Yet, the algorithm is still verifying hailstorms, which will all turn out to be false alarms in the algorithm's final output. These time lapses warrant enough consideration to be thought of as non-hail days, given the quantity of volume scans between the verified hail occurrences within the data set.

2) ALGORITHM OUTPUT

The next step is running the hail algorithm, which uses level II radar data that generates an output file for each day. This file consists of the locations and SHI values of all storm cells detected by the SCIT algorithm, and is organized by volume scan

number. However, the detection of numerous smaller-scale cells within a larger, multi-celled storm can overload the output file and give muddled results. Therefore, an adaptable parameter within WATADS allows the user to select a minimum separation distance between detected cells. This allows only the dominant cell within a multi-celled storm to be detected by the SCIT algorithm. This parameter is set to 10 km for this study.

3) HAIL-TRUTH FILE AND TIME WINDOWS

After the algorithms are run using the radar data, the next step is to set up a hail-truth file for each day studied. This file relates the actual hail reports to the storm cells observed by the algorithm. It accomplishes this by recording the time and location of the cell that produced the verified hail report for each volume scan. Since the only hail verification in this study is via *Storm Data*, and since its precision in the spatial and temporal is not the best, a time window is introduced into the hail-truth file to reduce this inaccuracy. This was done by recording the time and location of a cell that is associated with a hail report both before and after the time of the report. For this study a time window of 20 minutes was used for each hail report recorded in the hail-truth file. This was based on a time-window methodology used by Witt et al. (1998) in his analysis of the hail algorithm.

Witt's time window was 20 minutes in length and looked 15 minutes prior and 5 minutes after the recorded hail report. This time length was chosen based on the time taken for large hail to fall out of a storm (Changnon 1968). The actual time is 10 minutes, but a five-minute buffer was added to both sides of the window to account for synchronization errors between the radar and the observed hail report. Table 2 shows an example of a hail-truth file used for this study, illustrating the 20-minute time window.

4) ALGORITHM SCORING AND STATISTICS

The scoring of the algorithm is a three-part process. First, a fortran program is used to compare the hail-truth file with the output file. This program takes each line of the hail-truth file and matches it to a corresponding line (by time and location) in the output file. When running the program, the user must input a wide range of warning threshold (WT) values. Depending on certain threshold values, the program detects and tabulates a hit, miss, or false alarm for severe hail, and places this information in a separate output file. The next step in the process involves running another fortran program on the newly formed output file that finds and eliminates duplicate lines in the output.

After the first two parts are successfully completed, the final part of the scoring involves computing the statistical performance results of the algorithm. The algorithms are evaluated using the POD (Probability Of Detection), FAR (False Alarm Ratio), and CSI (Critical Success Index) statistics (Wilks 1995). Table 3 defines these values.

5) POSH RELIABILITY

After the algorithm scoring is completed, the next step is to look at the overall reliability of the algorithm. The reliability of this algorithm is determined by comparing the POSH values with the observed relative frequency (ORF) of each hail event. For example, suppose one forecasts rain for a particular region for 10 days and all of the forecasts call for a 30% probability of rain. Now, suppose that observations show that rain occurred only 2 out of the 10 days. The ORF would be the frequency of the actual observed event, or 20%. This demonstrates the reliability of the forecasts and shows that the predictions are higher (30%) than the observations, thereby leading to a small over-forecasting bias.

Calculating the reliability of the POSH algorithm is slightly more complicated. As stated before, the hail observations in *Storm Data* are not very dependable and only represent a small portion of the hail event. Therefore, it is necessary to use the time-

Table 2. The partial hail-truth file for hail reported on 03 November 1995. The value on the first line is the number of hail reports for that day. The second line indicates the size of hail and the time in which it was reported. The following lines indicate the storm locations for the volume scans ~15 minutes before the report and ~5 minutes after the report, giving a 20-minute time window for verification.

9 [# of hail reports]		
19 [size (mm) of hail]	0450 [time (Z) of report]	
Azimuth (°)	Range (km)	Volume Scan Time (Z)
354	156	0433
355	159	0439
356	162	0445
358	166	0451
359	169	0457

Table 3. 2X2 contingency table of forecast versus observed states, used to determine statistical skill scores for Y (yes) / N (no) predictions of an event. POD is the likelihood that the event would be forecast, given that it occurred. FAR is the proportion of forecast events that fail to materialize. CSI is the number of correct "yes" forecasts divided by the total number of occasions on which that event was forecast and/or observed.

	Forecast Event	Forecast No Event	Total
Observed Event	YY (Hit)	YN (Miss)	YY+YN
Observed No Event	NY (False Alarm)	NN	NY+NN
Total	YY+NY	YN+NN	

Where:

$$POD = \frac{YY}{YY + YN} \qquad FAR = \frac{NY}{YY + NY} \qquad CSI = \frac{YY}{YY + NY + YN}$$

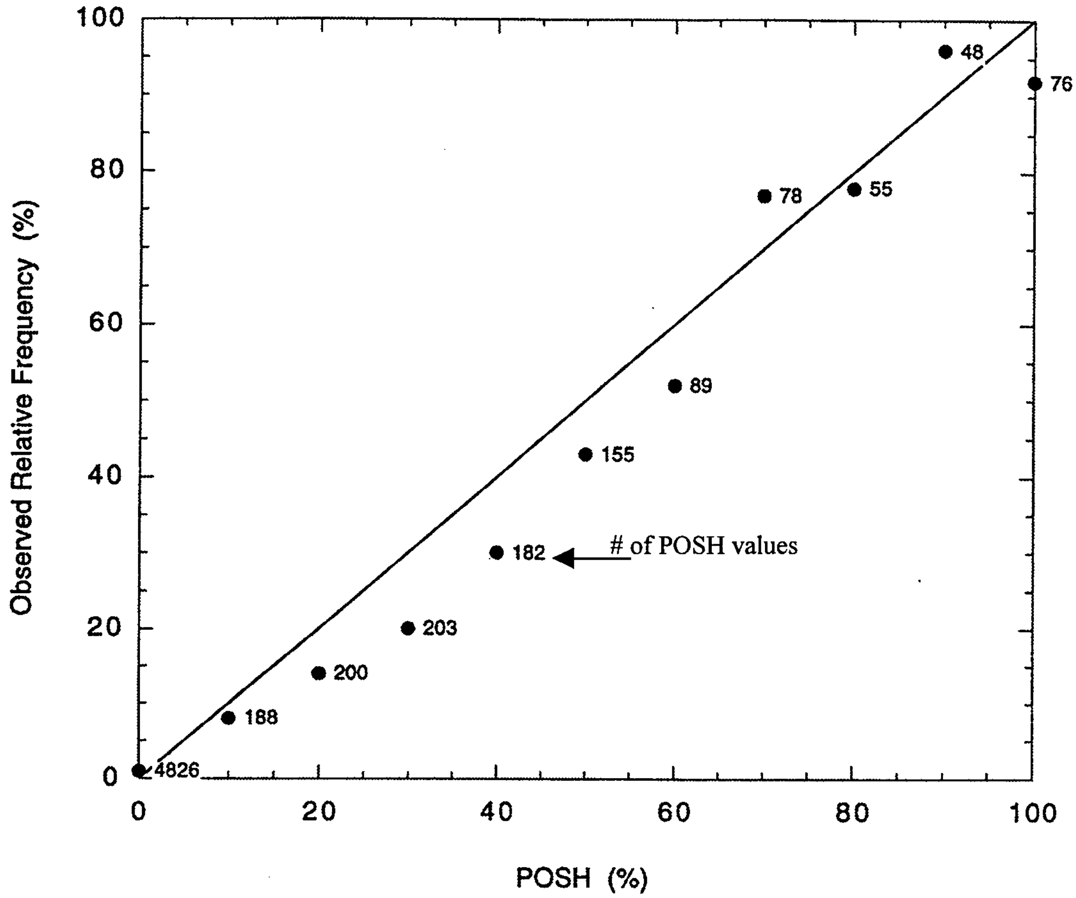

Figure 5. Reliability diagram for the probability of severe hail for 10 days of radar data from Oklahoma and Florida. The numbers adjacent to the plotted points indicate the number of forecasts for a particular POSH value. The x-axis represent the forecasted POSH values, while the y-axis represent the observed relative frequency of the severe hail occurrence. The diagonal line represents perfect reliability. Adapted from Witt et al. (1998).

window methodology to increase the number of hail reports (observations) that will be associated with a specific hail prediction. So, in order to calculate the ORF values for POSH, it's simply a matter of determining the number of times, for each POSH category, that these observations occur within the time window compared to the total number of predictions. For example, if one analyzes a day that has a total of 100 POSH predictions at 40%, and 25 of these predictions occur within the time window allotted for each hail report, then the ORF will be 25% for the 40% POSH category. Therefore, the reliability of the POSH algorithm shows an over-forecasting bias at POSH=40%. Figure 5 shows an example of a POSH reliability diagram for a NSSL hail study using 10 days of radar data from Oklahoma and Florida. Notice the over-forecasting bias from POSH values from 10% through 60%.

6) OPTIMIZING THE WTSM

One of the inputs to the POSH equation is the warning threshold (WT) which depends of the height of the melting layer according to the WTSM (Eq. 6), where WT is the Warning Threshold and H_0 is the height (in km) of the melting layer. The WTSM was derived primarily from springtime hail events in the Southern Plains and Florida (Witt et al. 1998). Since the WTSM was developed in a different region, an adjustment to the equation for different environments may be required.

For each hail event, there exists an optimum warning threshold that produces the highest CSI. This can be plotted against the melting layer of the day to produce a new, more accurate WTSM for the League City area. A graphical example can be found on Figure 6. This comes from the same NSSL hail study used to show the reliability graph on Figure 5. The parameters within Eq. (6) that can be adjusted are the y-intercept value (-121) and the slope value (57.5). Local soundings from Corpus Christie, TX and Lake Charles, LA will provide the necessary melting layer values.

The optimum warning threshold is determined for each hail day when scoring the algorithm. This is done by entering a wide range of warning threshold (WT) values into the scoring algorithm, and choosing the one WT value that leads to the highest CSI.

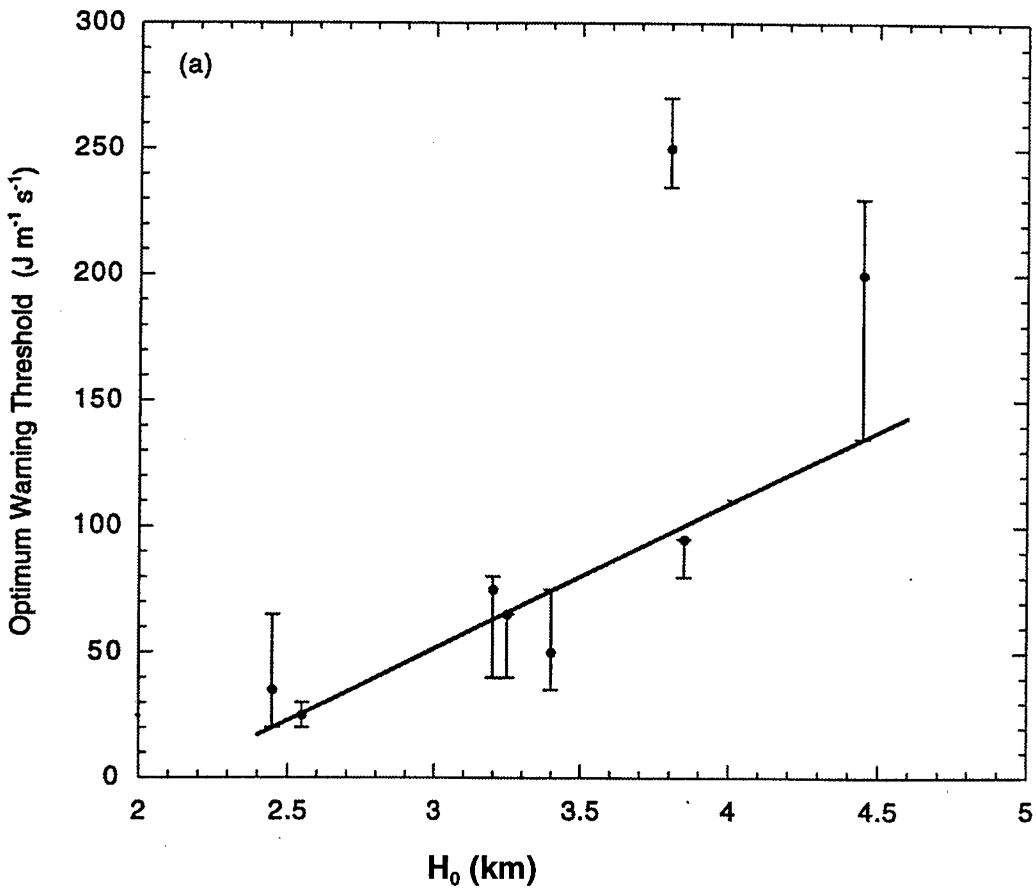

Figure 6. This figure shows the optimum warning threshold (black line) as a function of the melting layer from the initial HDA tests made by NSSL. The solid circles correspond to the highest CSI. The vertical bars represent the range of warning threshold values within 5 percentage points of the maximum value. Adapted from Witt et al. (1998).

Recalling equation (1) shows that the probability equation for POSH involves a direct ratio between the SHI value (computed for every storm cell and volume scan) and the WT value. The scoring algorithm declares a "yes" forecast for severe hail if the SHI value is greater than or equal to the WT value; otherwise a "no" forecast for severe hail is made. Depending on the WT value given, the POD, FAR and CSI values can change. Table 4 shows an example of the algorithm's performance results for 09 September 1997. Here, the highest CSI value of 35 corresponds to a WT value of 120. Given the melting level for the day, this WT value can now be plotted as one of 18 points. Finally, a new WTSM line can be determined by ascertaining a "best fit" line from all data points.

7) POPULATION DENSITY CONSIDERATIONS

The accuracy of this algorithm's performance is dependent upon accurate and timely observations. Therefore, when looking to adapt this algorithm to a specific location, strong consideration should be made as to whether or not the population density has any effect on the reliability of the algorithm.

Wyatt and Witt's (1997) study showed that in some locations the reporting of hail is better in areas of high population density than in areas where there are few people to report it. Therefore, the analysis of a hail detection algorithm's performance as a function of population density may effectively reduce the number of "false alarms" generated by the algorithm, thereby increasing its CSI score. This finding is interesting for this study due the fact that Harris County, which includes the city of Houston, has an average population density of 630 persons per km^2. This is in direct contrast to both Grimes and San Jacinto counties, adjacent to Harris County, whose average population densities are equivalent to approximately 10 persons per km^2.

The population density program works in the same way as the original algorithm scoring program, with some minor differences. The population density program

Table 4. Performance results from the hail algorithm for 09 September 1997 using the 20-minute time window. WT is the warning threshold. Here, the highest CSI value (35) corresponds to a warning threshold value of 120. The POD, FAR, and CSI values are all in percent.

WT	**Hits**	**Misses**	**False Alarms**	**POD (%)**	**FAR (%)**	**CSI (%)**
80	16	7	29	70	64	31
90	15	8	25	65	63	31
100	15	8	24	65	62	32
110	14	9	22	61	61	31
120	14	9	17	61	55	35
130	11	12	16	48	59	28
140	11	12	13	48	54	31
150	11	12	12	48	52	31
160	10	13	10	43	50	30
170	9	14	9	39	50	28

includes a data set, which contains the entire population density of the League City radar coverage area. This data comes from the 1990 census and was obtained from the Socioeconomic Data and Applications Center (1995). The data were averaged into a 2km-by-2km grid, thus containing $4km^2$ squares of data.

After these values are read into the program, it then asks for a population density threshold value. Using this threshold value, the scoring program runs the same as the original, but excludes scoring in all areas that fall below the threshold value. After systematically testing different threshold values, one value should lead to an optimum algorithm performance score. This optimum score can be depicted by graphing the population density threshold values versus the scoring values of POD, FAR, and CSI. This optimization technique should decrease the number of false alarms that the algorithm reads and ultimately produce a better reliability score.

8) OPTIMIZING THE POSH PROBABILITY EQUATION

Finally, after the variables of the new WTSM and the values of the optimum population density threshold are determined, they can be placed back into the algorithm and run again for the 18 hail days. Statistical values should indicate an increase in the CSI, as the WTSM would be optimized for the League City radar. After ascertaining the new optimum CSI values, a new reliability graph can be plotted. This should reveal an increased reliability in the algorithm, as it will be more adapted to the NWS League City County warning area.

However, another way to obtain an optimized HDA is to directly adjust the parameters of the POSH probability equation (1). This equation is essentially a linear function relating the probability of severe hail to the logarithmic value of the severe hail index normalized by the warning threshold for that day. The equation contains two constants, the slope and intercept parameter of the linear relationship. Either parameter can be adjusted. Hence, a straight forward adjustment to the HDA would be to alter either the intercept or the slope parameter in the equation in order to obtain reliability results closer to the optimum.

9) SENSITIVITY TO RADAR CALIBRATION

The League City radar was recalibrated after February 1998. It was found that the radar was under-computing storm reflectivities by close to 2 dBZ. This can sometimes happen as radar technicians attempt to lengthen the life-span of the radar by decreasing the power at which the radar operates. However, doing this has the ill effect of having the radar under-compute storm reflectivities.

Since the entire data set from this study occurred before January 1998, a sensitivity test will be done on a sub-set of the data to ascertain whether or not this error has any effect on the reliability and the performance of the POSH equation.

CHAPTER IV

RESULTS

The methodology described in the previous section was used with the data available for the League City county warning area from April 1994 through January 1998. These results provide preliminary information on the NSSL POSH algorithm over the League City NWS office area of interest. The first section will briefly summerize the results from a recent NSSL hail algorithm study, which studied the algorithm's performance over different regions of the United States. The second section will present the results from this hail study, and then compare these results with those from the NSSL study.

a. NSSL hail study results

To provide an independent test of the SHI value, the initial WTSM, and the initial POSH probability function, NSSL performed an extensive study on their hail algorithm. This study included storm data from 31 days and 7 different radar across the United States (Witt et al. 1998). Table 5 lists all the radar locations used, along with the definitions of the separate regions. From the regions tested, the League City forecast area would most likely fall under the Mississippi River or the Southern Plains region.

The default WTSM was used on these data to run the hail algorithm and produce performance statistics. Table 6 reveals these regional performance results. The SP region appears to have the highest scoring statistics. This is probably due to the fact that the default WTSM was developed using data mostly from this area. Also, data from this region account for over 60% of the overall data from this study.

The smallest variation throughout the regions appears to be in the POD value, having a range size of 11 percentage points. This is in direct contrast to the FAR and CSI values, having ranges of 29 and 35 percentage points, respectively. One possibility for this might be that the original WTSM is not highly representative of these different

Table 5. This table shows the regions used for the NSSL hail algorithm study. NHD represents the number of hail days used in the data set from that region. NR represents the number of hail reports used in the data set from that region. The three-letter radar identifiers are included after the radar location. From Witt et al. (1998).

Region	NHD	NR	Radar Location (ID)
Southern Plains	7	222	Dodge City, Kansas (DDC)
			Norman, Oklahoma (OUN)
			Twin Lakes, Oklahoma (TLX)
Florida	10	32	Melbourne, Florida (MLB)
Mississippi River	9	70	St. Louis, Missouri (LSX)
			Memphis, Tennessee (NQA)
Northern US	4	30	Milwaukee, Wisconsin (MKX)
			Minneapolis, Minnesota (MPX)
			New York City, New York (OKX)
Total	**31**	**364**	

Table 6. Regional performance results for the NSSL study. From Witt et al. (1998).

Region	Overall POD (%)	Overall FAR (%)	Overall CSI (%)
Southern Plains	**82**	**54**	**41**
Florida	**71**	**75**	**23**
Mississippi River	**80**	**83**	**16**
Northern United States	**71**	**58**	**36**
Average from all regions in NSSL study	**78**	**69**	**29**

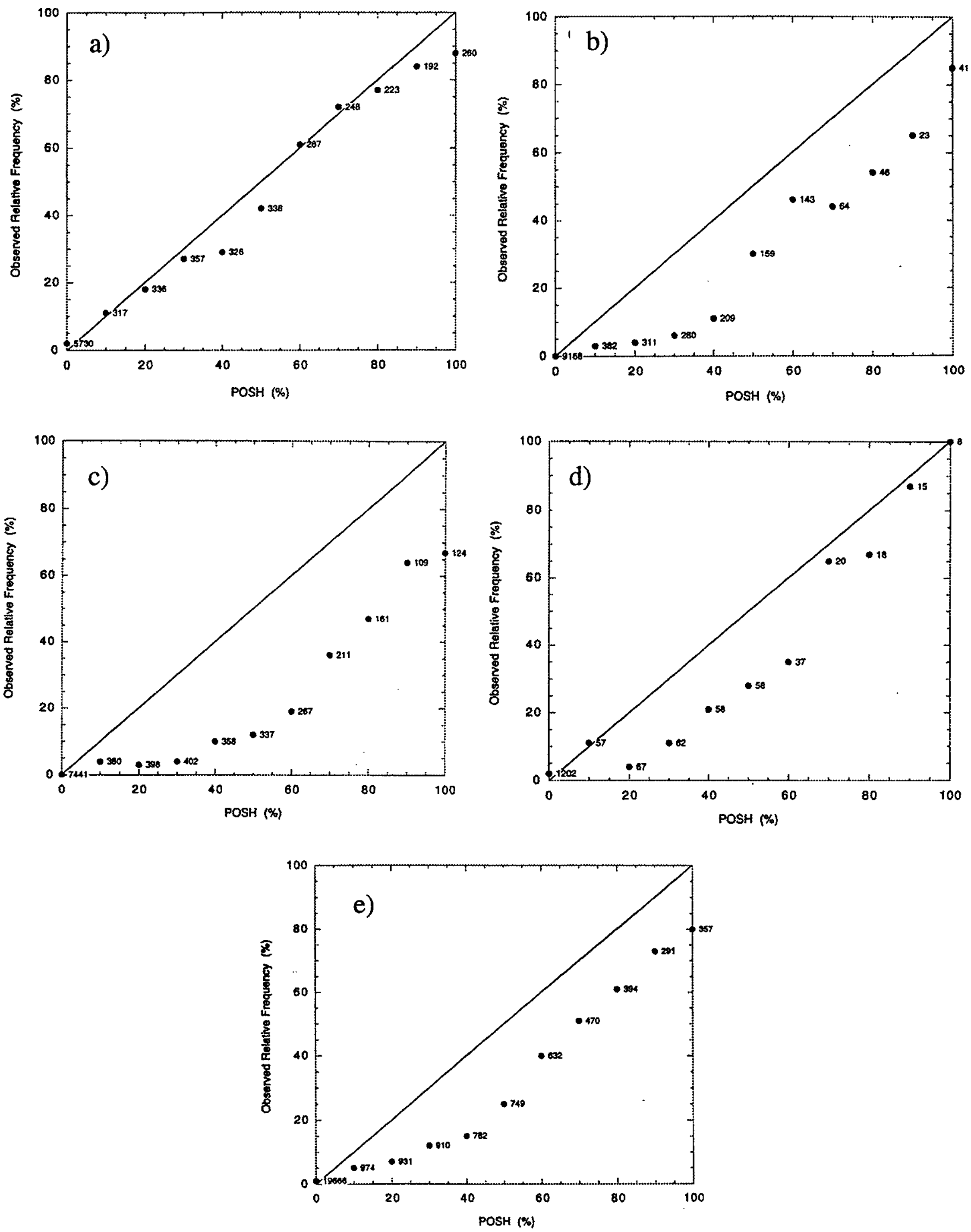

Figure 7. Same as Figure 5, but data comes from regional NSSL study performed over 31 storm days and 7 radar locations. The regions are labeled as follows: a) southern plains, b) Florida, c) Mississippi River, and d) northern United States. Part e) represents the average reliability of Figures 9a through 9d. Adapted from Witt et al. (1998).

regions. Since the WTSM was developed using radar data from Oklahoma and Florida, this is a distinct possibility.

To evaluate the POSH parameter, reliability diagrams were made to show the algorithm's performance over these regions. Figures 7a through 7d show the algorithm's reliability in the separate regions tested, while Figure 7e shows the average reliability of the algorithm in all regions. As stated before, the League City forecast area would most likely fall within the Southern Plains region, Figure 7a, or the Mississippi River region, Figure 7c.

b. League City hail performance results

Following after the methods used by the NSSL study, the HDA was tested for accuracy over the League City warning area. After analyzing the results from the NSSL study, the next step was to tabulate statistical data for the League City county warning area, and then compare those results with the results from the NSSL test. For the 18 hail days, the algorithm was run using the default WTSM values as determined by NSSL. The algorithm results from the League City data run are shown Tables 7 and 8. Table 7 breaks up the data into storm forcing mechanisms: seabreeze and continental. The performance statistics from the seabreeze data appear to be good, but should not be fully trusted due to the fact that of the 120 hail reports used, only 15 of them were due to convection triggered by a seabreeze front (see Table 1). The CSI results from the continental data were lower compared with the overall averages, but this is due to the increased number of false alarms within the data. Table 8 breaks up the data into seasons of the year, where the Fall/Winter months make up 33% of the hail reports. Surprisingly, the Fall/Winter months, where there are not as many hail reports, show better algorithm performance than the Spring/Summer months.

When compared with the regional results from the NSSL experiment, the League City study produces lower values for POD, but a comparable value for the CSI. These results show that the default parameters for both the WTSM

Table 7. Data analyzed from the League City radar. **H** is a hit, **M** is a miss, and **FA** is a false alarm.

Seabreeze Data								
Date	**H_0 (km)**	**WT**	**H**	**M**	**FA**	**POD**	**FAR**	**CSI**
3 Jun 96	4.50	138	7	1	4	88	36	58
2 Jun 96	4.29	126	4	4	0	50	0	50
4 Jun 96	4.14	117	2	18	3	10	60	9
21 May 97	4.35	129	2	1	2	67	50	40
2 Sep 97	4.30	126	1	1	2	50	67	25
Average from Seabreeze Events						**39.02**	**40.74**	**30.77**

Continental Data								
Date	**H_0 (km)**	**WT**	**H**	**M**	**FA**	**POD**	**FAR**	**CSI**
21 Jan 98	3.98	108	14	9	18	61	56	34
22 Jan 98	3.96	107	22	22	33	50	60	29
9 Sep 97	4.60	144	11	12	13	48	54	31
3 Nov 95	4.15	118	6	17	8	26	57	19
25 Apr 97	3.72	93	8	8	9	50	53	32
11 Apr 97	3.70	92	12	18	7	40	37	32
28 May 97	4.10	115	4	4	7	50	64	27
2 May 94	3.96	107	15	5	5	75	25	60
5 Apr 94	4.23	122	10	7	17	59	63	29
15 Apr 94	4.08	114	12	17	37	41	76	18
11 May 95	4.53	140	8	19	23	30	74	16
27 Apr 97	4.42	133	2	23	5	8	71	7
5 Apr 96	3.80	98	19	18	27	51	59	31
Average from Continental Events						**44.41**	**59.38**	**26.93**
Overall Average from League City Study						**43.80**	**58.05**	**27.27**

Table 8. Same as Table 7, except data is divided by time of occurrence, namely either Spring/Summer or Fall/Winter.

Spring/Summer Data								
Date	**H_0 (km)**	**WT**	**H**	**M**	**FA**	**POD**	**FAR**	**CSI**
3 Jun 96	4.50	138	7	1	4	88	36	58
2 Jun 96	4.29	126	4	4	0	50	0	50
4 Jun 96	4.14	117	2	18	3	10	60	9
21 May 97	4.35	129	2	1	2	67	50	40
25 Apr 97	3.72	93	8	8	9	50	53	32
11 Apr 97	3.70	92	12	18	7	40	37	32
28 May 97	4.10	115	4	4	7	50	64	27
2 May 94	3.96	107	15	5	5	75	25	60
5 Apr 94	4.23	122	10	7	17	59	63	29
15 Apr 94	4.08	114	12	17	37	41	76	18
11 May 95	4.53	140	8	19	23	30	74	16
27 Apr 97	4.42	133	2	23	5	8	71	7
5 Apr 96	3.80	98	19	18	27	51	59	31
Average from Spring/Summer Events						**42.34**	**58.17**	**26.65**

Fall/Winter Data								
Date	**H_0 (km)**	**WT**	**H**	**M**	**FA**	**POD**	**FAR**	**CSI**
2 Sep 97	4.30	126	1	1	2	50	67	25
21 Jan 98	3.98	108	14	9	18	61	56	34
22 Jan 98	3.96	107	22	22	33	50	60	29
9 Sep 97	4.60	144	11	12	13	48	54	31
3 Nov 95	4.15	118	6	17	8	26	57	19
Average from Fall/Winter Events						**46.95**	**57.81**	**28.57**

and the POSH probability function create CSI statistics equivalent to those of the NSSL study, and thereby could be considered accurate for the League City warning area. However, another way to test the accuracy of the HDA is to determine whether or not the WTSM remains highly correlated with the melting level. If so, then optimizing the WTSM parameters will be the next objective.

1) WTSM GRAPHS

For each day listed on Table 7, an optimum warning threshold was determined using the scoring programs. This data was plotted against the melting level of the day. Since the performance results were divided into different classifications, so too were the data for the WTSM graphs. This is shown on Figures 8a through 8h. The seabreeze data appears to show a well-correlated WTSM line. However, these results are suspect due to the lack of data. As well, the Spring/Summer data appears to be more correlated than does the Fall/Winter data.

The Spring/Summer data were further separated by continental and seabreeze convective forcing. This proved to be useful as the continental-Spring/Summer data were highly correlated. This was also useful because half of the data set was contained in this subset. The seabreeze-Spring/Summer data was also highly correlated, but again, the lack of data lessens the credibility of the results. Lastly, separating the continental-Fall/Winter data showed relatively no correlation.

After analyzing the results from these graphs, the next step was to select a new WTSM to use in the final analysis of the NSSL hail algorithm. The line with the highest correlation could be used, but this appears in the seabreeze data (Figure 8b), where data points are few. This eliminates the usage of the seabreeze and seabreeze-Spring/Summer (Figure 8f) plots. Another consideration has to do with the limilations of the WATADS software. When inputting new parameters into the hail algorithm, WATADS only allows a window of –500 to +500 for the y-intercept value. This disallows another highly correlated plot, the continental-Spring/Summer plot (Figure 8e), with a correlation of .83. Therefore, the slope and y-intercept values from the

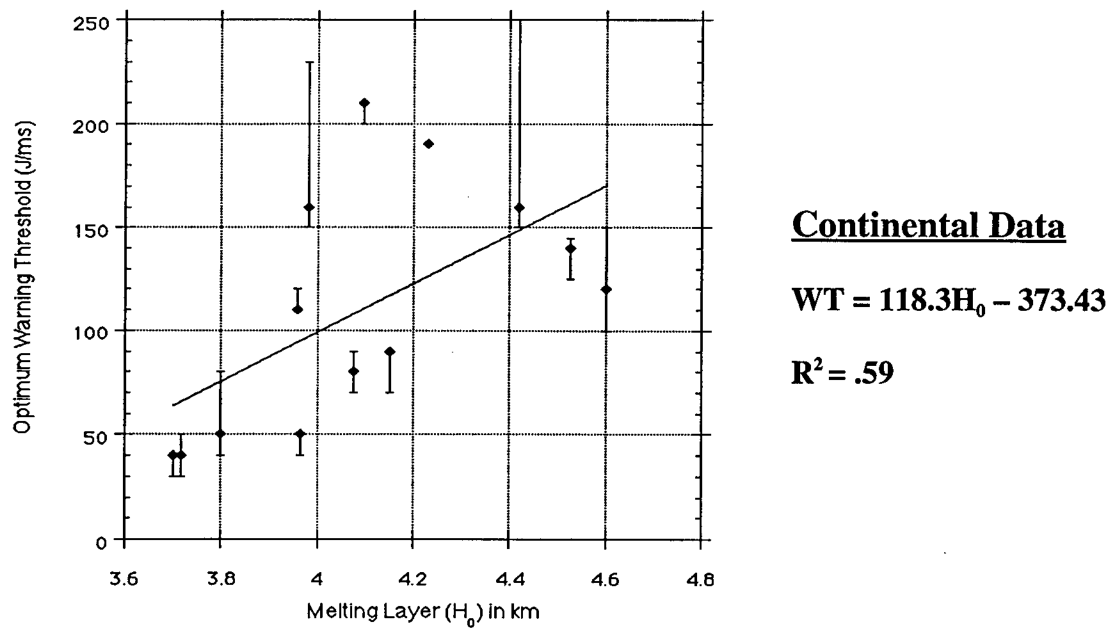

Figure 8a. WTSM plot for all continental-forced hail days. The black line represents the "best fit" linear correlation of the data, which is shown numerically to the left of the plot. The R^2 value represents the correlation value of this line.

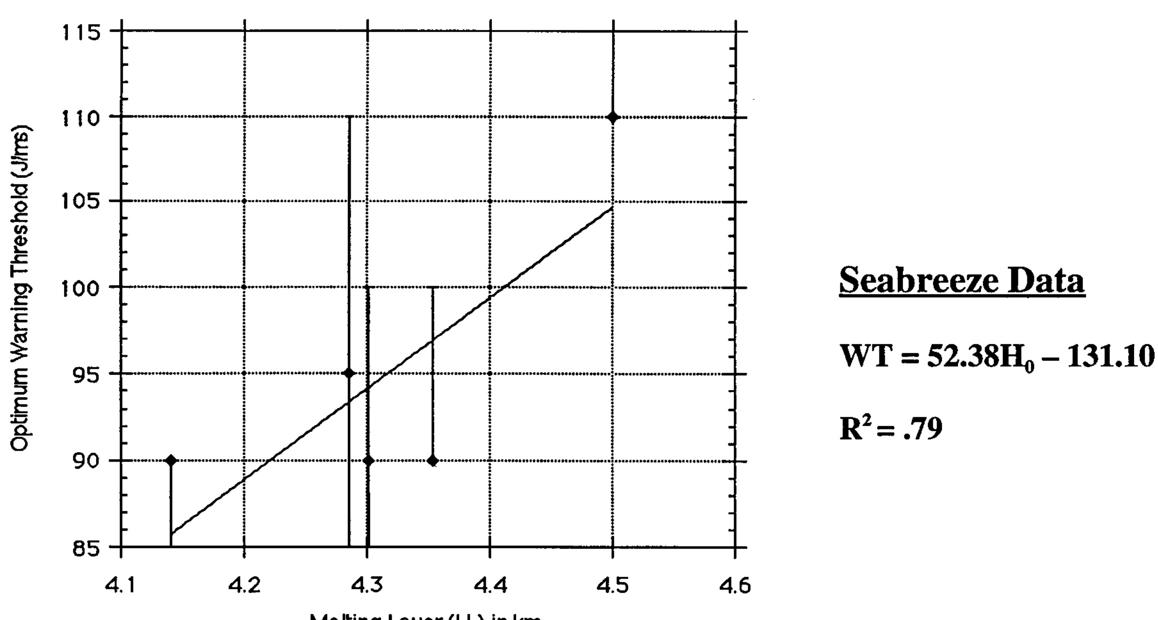

Figure 8b. Same as Fig. 8a, but for all seabreeze-forced hail days.

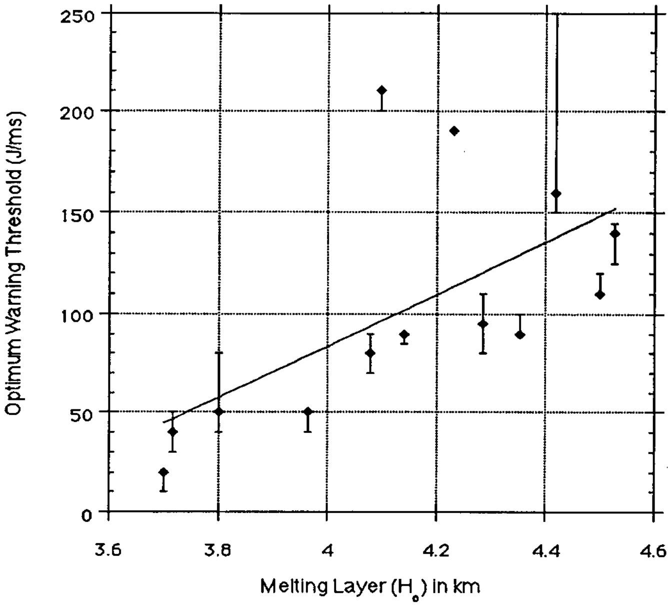

Spring/Summer Data

$WT = 130.43H_0 - 435.0$

$R^2 = .63$

Figure 8c. Same as Fig. 8a, but for all Spring/Summer hail days.

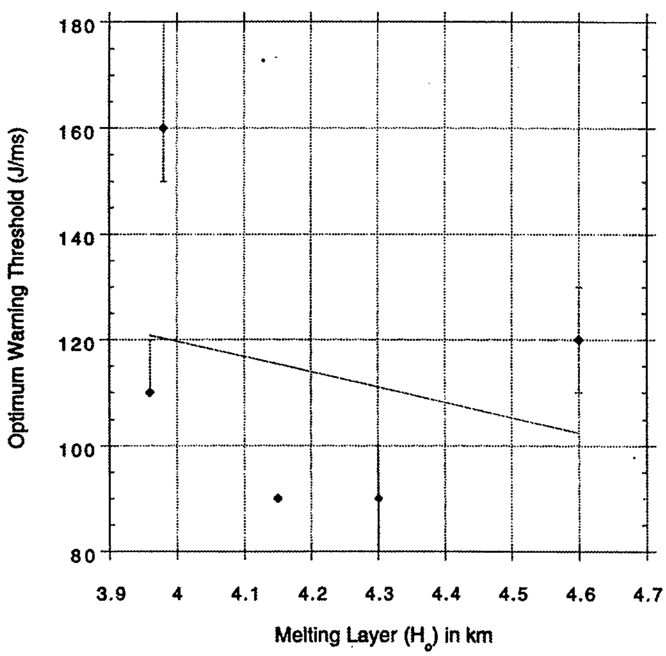

Fall/Winter Data

$WT = -28.65H_0 + 234.27$

$R^2 = .26$

Figure 8d. Same as Fig. 8a, but for all Fall/Winter hail days.

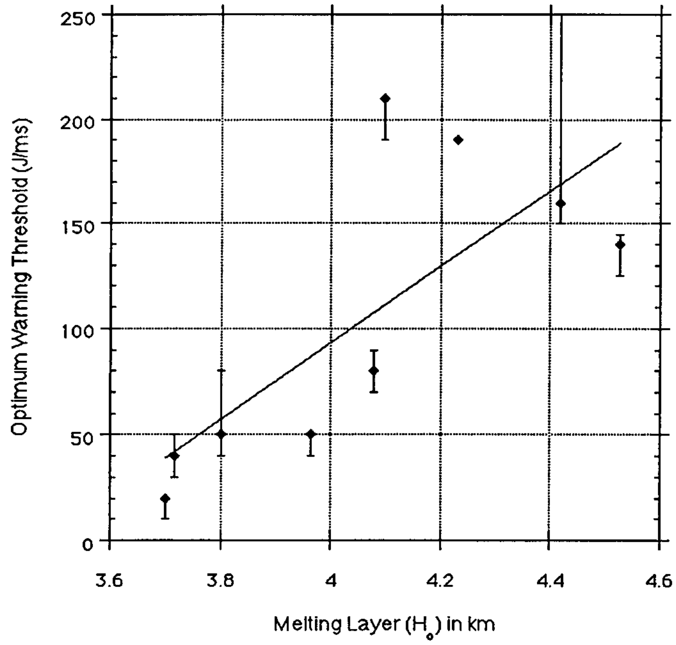

Cont-Spr/Sum Data

$WT = 180.51H_0 - 628.21$

$R^2 = .75$

Figure 8e. Same as Fig. 8a, but for all continental Spring/Summer hail days.

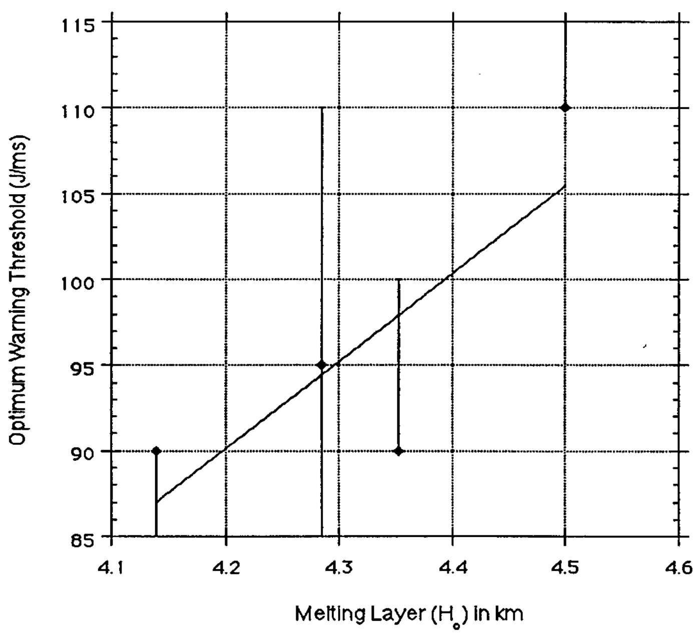

Sea-Spr/Sum Data

$WT = 51.22H_0 - 124.99$

$R^2 = .81$

Figure 8f. Same as Fig 8a, but for all seabreeze-Spring/Summer hail days.

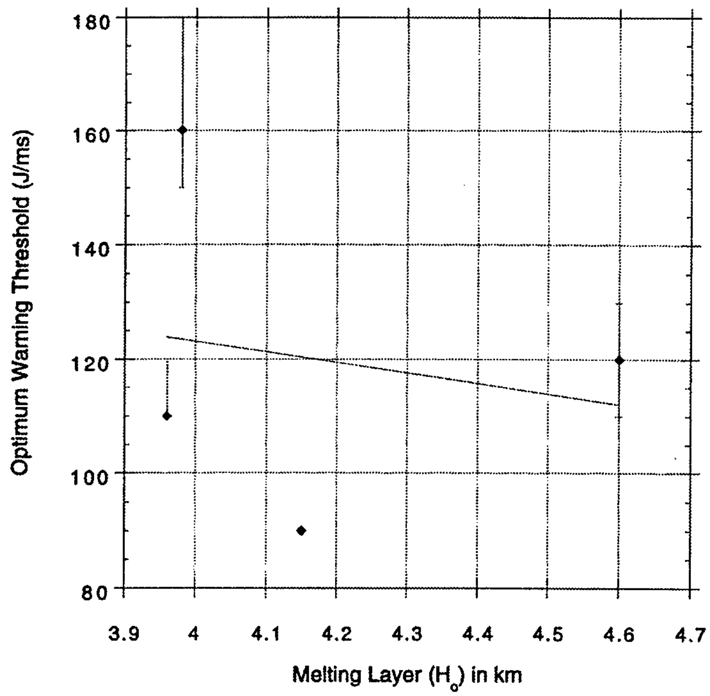

Cont-Fall/Wint Data

$WT = -18.46H_0 + 197.01$

$R^2 = .19$

Figure 8g. Same as Fig. 8a, but for all continental-Fall/Winter hail days.

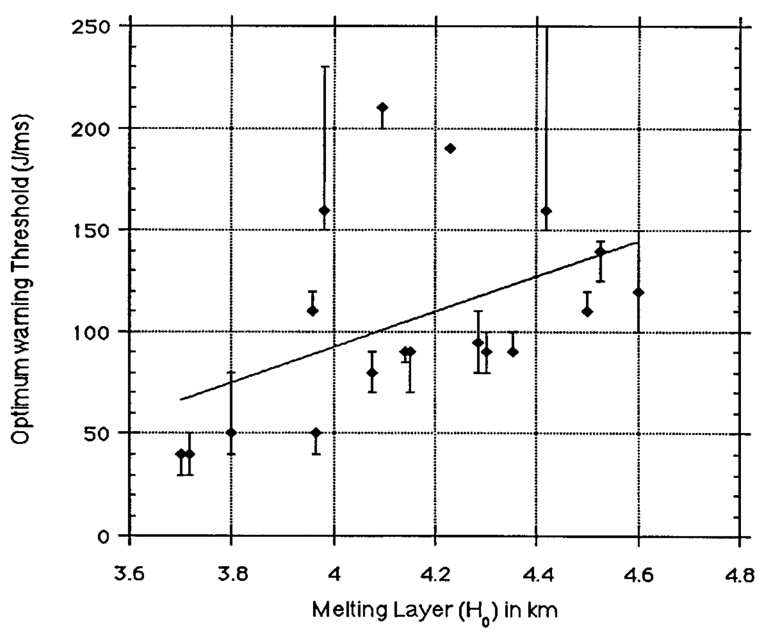

All Data

$WT = 87.67H_0 - 257.9$

$R^2 = .48$

Figure 8h. Same as Fig 8a, but for all 18 hail days.

Spring/Summer plot, with a correlation of .73, will be used to analyze the hail algorithm for the League City warning area. These WT values are shown on Figure 8c.

2) POSH RELIABILITY

Another way to test the accuracy of the hail detection algorithm over the area of study is to plot the reliability of the POSH equation. To accomplish this, the specific POSH values were tabulated into two categories; predicted POSH values from the algorithm output files and actual POSH values from the hail-truth files. These data were then compared with each other and placed onto a reliability graph, which is shown on Figure 9. From this graph, one can see an over-forecasting bias by the algorithm for every POSH value. Also, the reliability seems to worsen after 80%. However, this is due to the lack of observations at both 90% and 100%. A simple cumulative distribution graph (Figure 10) shows this to be true. The forecasted values of POSH from 10 to 80 account for 98% of the data. Therefore, the results shown for the last two POSH values are based on a data sample too small to be counted as significant.

Most of the data points appear to be progressing at a linear rate, suggesting that, as well as testing a new WTSM, it also may be useful to parameterize the offset parameter of the POSH probability function using the default WTSM.

3) POPULATION DENSITY CONSIDERATIONS

Before the hail algorithm was run using the new parameters, the issue of a population density bias in the data was addressed. Using the findings and threshold values from Wyatt and Witt (1998) concerning population density bias, a special program was run that filters out data below certain population density thresholds. The thresholds, in units of persons per $4km^2$, used for this study are listed as follows: 0, 100, 250, 500, 750 and 1000. Figure 11 shows the results from running the hail algorithm with the population restrictions. The results from this exercise show the highest CSI and POD values appear when there are no population restrictions on the data. Wyatt

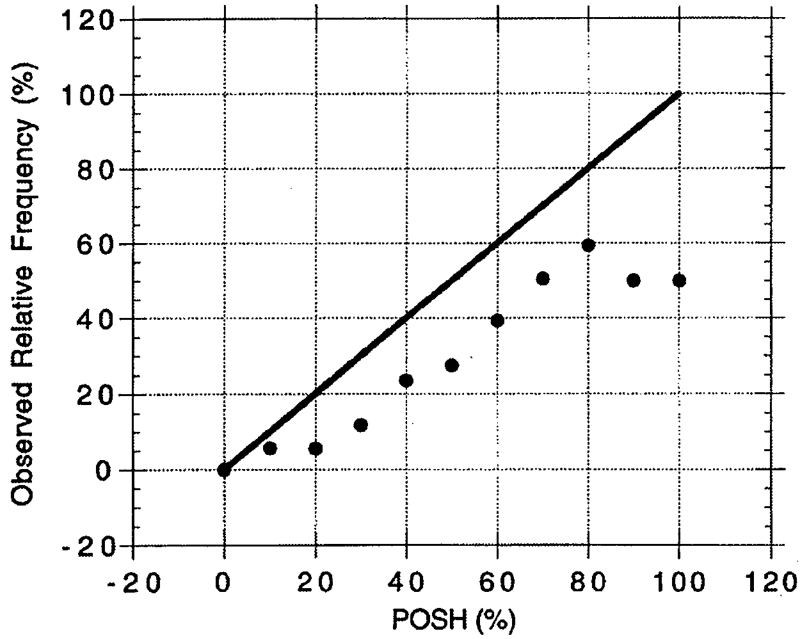

Figure 9. This is the reliability graph for the League City county warning area using only the default algorithm values. The solid black line represents the optimum reliability. The circles represent the actual reliabilities of each POSH value.

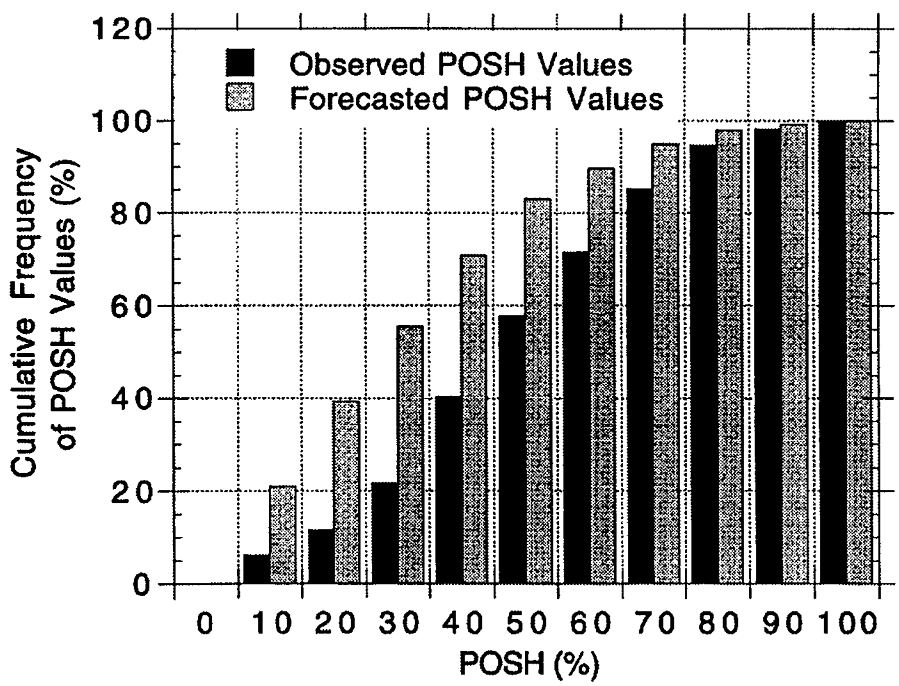

Figure 10. This is a graph showing the cumulative frequency distributions of both the observed and forecasted POSH values. The default algorithm parameters were used to calculate this data.

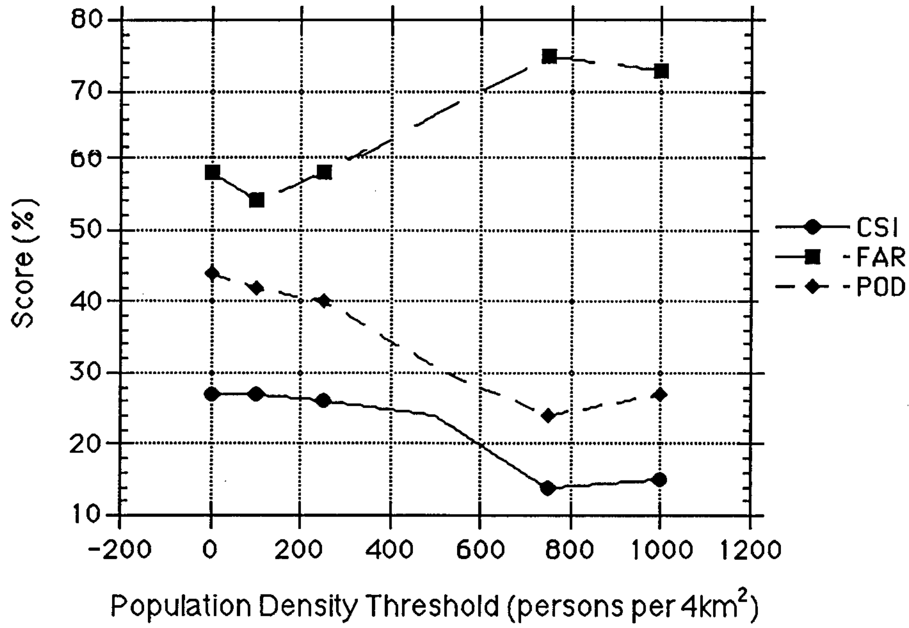

Figure 11. This figure shows the statistical scoring values plotted against certain population density thresholds.

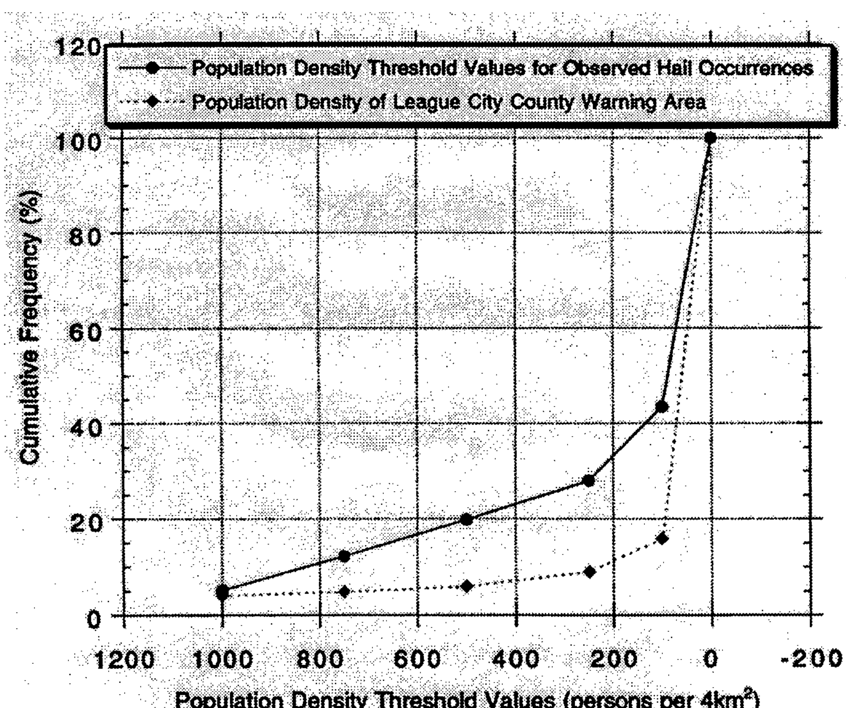

Figure 12. This figure shows the cumulative frequency distribution of the observed hail occurrences based on population density threshold values versus the population density distributions over the League City county warning area.

and Witt (1998) came across this in their study as well. They examined two radar locations: Melbourne, Florida and Fort Worth, Texas. In the Florida case they saw maximum performance statistics at the 1000 persons per $4km^2$ point. However, the Fort Worth case showed the best hail performance statistics at 0 persons per $4km^2$.

The reason for this behavior is most likely in the data-gathering process itself. Wyatt and Witt (1998) claimed that the reason the Fort Worth data behaved as it did was due to the fact that most of the hail reports were from rural areas (less than 100 persons per $4km^2$). A cumulative frequency distribution of hail reports sorted by population density over the League City county warning area (Fig. 12) illustrates this for the current study to some point. The distribution of hail reports can be compared to the fractional area of the county warning area covered by each increment in population density threshold (the dashed curve in Fig. 12). Close to 85% of the total area within this county warning area have population densities $\leq$ 100 persons per $4km^2$. However, only approximately 55% of the observed hail occurrences for this study occurred within this population threshold. Other thresholds on the graph point to the same conclusion — that there is a likelihood that the gathering of hail reports solely from *Storm Data* will tend to bias the hail-truth file towards more largely populated areas. While expected, this illustrates the difficulty in obtaining validation information that is representative of the natural variability of hail events. With most of the hail reports for this study coming from rural areas, testing for an optimum population density threshold proved unfruitful in lessening the FAR for a more reliable score.

4) OPTIMIZED WTSM RESULTS

The statistical results from running the hail algorithm with the new WTSM are presented on Tables 9 and 10. There is an increase in the CSI and POD values, and a decrease in the values for FAR. This statistical increase may indicate that the default WTSM parameters were not optimal over the League City data set. Using the new WTSM, a new reliability graph was plotted and is shown on Figure 13. This shows a good improvement of the algorithm for the 0% to 40% POSH values. From 40% to 60% the new reliability is better than the old, but there is still a distinct over-forecasting

Table 9. Same as Table 7, except this table shows the statistical results from running the hail algorithm using an optimized WTSM line.

Seabreeze Data								
Date	**H_0 (km)**	**WT**	**H**	**M**	**FA**	**POD**	**FAR**	**CSI**
3 Jun 96	4.50	150	7	1	4	88	36	58
2 Jun 96	4.29	123	4	4	0	50	0	50
4 Jun 96	4.14	103	4	16	9	20	69	14
21 May 97	4.35	131	2	1	0	67	0	67
2 Sep 97	4.30	124	1	1	0	50	0	50
Average from Seabreeze Events						**43.90**	**41.94**	**33.33**

Continental Data								
Date	**H_0 (km)**	**WT**	**H**	**M**	**FA**	**POD**	**FAR**	**CSI**
21 Jan 98	3.98	82	15	8	27	65	64	30
22 Jan 98	3.96	80	23	22	39	51	63	27
9 Sep 97	4.60	163	10	13	10	44	50	30
3 Nov 95	4.15	105	8	15	14	35	64	22
25 Apr 97	3.72	49	13	3	12	81	48	46
11 Apr 97	3.70	46	19	9	12	68	39	48
28 May 97	4.10	98	4	4	7	50	64	27
2 May 94	3.96	80	17	3	7	85	29	63
5 Apr 94	4.23	115	10	8	18	56	64	28
15 Apr 94	4.08	95	20	9	44	69	69	27
11 May 95	4.53	154	6	20	20	23	77	13
27 Apr 97	4.42	140	2	23	5	8	71	7
5 Apr 96	3.80	59	24	9	33	73	58	36
Average from Continental Events						**53.94**	**59.19**	**30.27**
Overall Average from League City Study						**52.79**	**58.00**	**30.53**

Table 10. Same as Table 8, except this table shows the statistical results from running the hail algorithm using an optimized WTSM line.

Spring/Summer Data								
Date	**H_0 (km)**	**WT**	**H**	**M**	**FA**	**POD**	**FAR**	**CSI**
3 Jun 96	4.50	150	7	1	4	88	36	58
2 Jun 96	4.29	123	4	4	0	50	0	50
4 Jun 96	4.14	103	4	16	9	20	69	14
21 May 97	4.35	131	2	1	0	67	0	67
25 Apr 97	3.72	49	13	3	12	81	48	46
11 Apr 97	3.70	46	19	9	12	68	39	48
28 May 97	4.10	98	4	4	7	50	64	27
2 May 94	3.96	80	17	3	7	85	29	63
5 Apr 94	4.23	115	10	8	18	56	64	28
15 Apr 94	4.08	95	20	9	44	69	69	27
11 May 95	4.53	154	6	20	20	23	77	13
27 Apr 97	4.42	140	2	23	5	8	71	7
5 Apr 96	3.80	59	24	9	33	73	58	36
Average from Spring/Summer Events						**54.55**	**56.44**	**31.96**

Fall/Winter Data								
Date	**H_0 (km)**	**WT**	**H**	**M**	**FA**	**POD**	**FAR**	**CSI**
2 Sep 97	4.30	90	3	0	0	100	0	100
21 Jan 98	3.98	110	13	9	13	59	50	37
22 Jan 98	3.96	160	22	22	21	43	37	35
9 Sep 97	4.60	120	14	9	17	61	55	35
3 Nov 95	4.15	90	8	15	14	35	64	22
Average from Fall/Winter Events						**52.18**	**52.00**	**33.33**

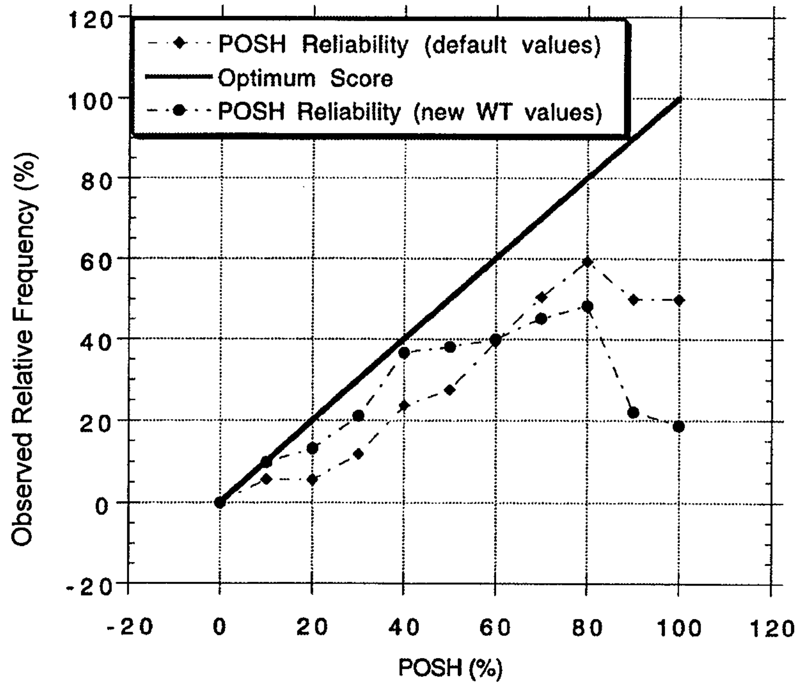

Figure 13. Same as Figure 9, except this figure includes the results from running the hail algorithm using the optimized WT values for the League City warning area.

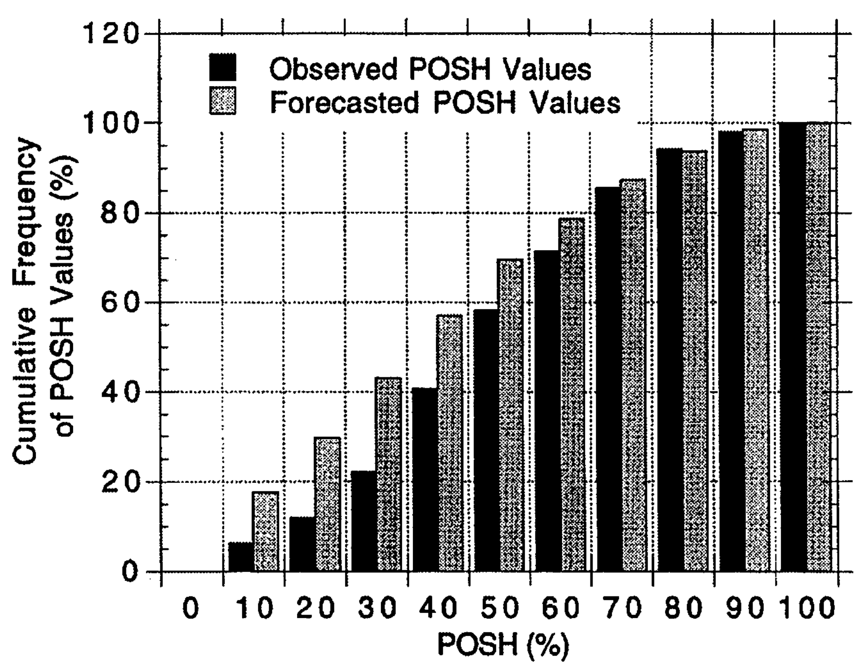

Figure 14. Same as Figure 10, except this figure shows the statistical results from running the hail algorithm using an optimized WTSM line.

bias. From 60% to 100% the new values are worse than the old, but this could be due to the limited number of POSH values greater than 60%.

The forecasted values of POSH from 10 to 60 account for 80% of the data, as shown by the cumulative distribution graph on Figure 14. Still, the bulk of the data is found between POSH values of 10% to 60%. It is not clear if the decrease in performance at the high end of the POSH values is associated with a lack of high quality validation data or an inherent limitation of the existing algorithm. Since testing the WTSM with the reliability graph is met with marginal success, the next step is to adjust the POSH probability function using the default WTSM values. This should produce similar results as optimizing the WTSM.

5) OPTIMIZING THE POSH PROBABILITY EQUATION

Visual inspection of the reliability graph (Figure 9) suggests that over most of the POSH range, the default algorithm over warned by about 20%. Hence, a straight-forward adjustment to the HDA would be to reduce the intercept parameter in the POSH equation by 20 so that:

$$POSH' = 29\ln\left(\frac{SHI}{WT}\right) + 30 \tag{7}$$

Where *POSH'* is the optimized value of POSH for this data set. All 18 hail days were run through the hail algorithm again using the new POSH equation.

The results are shown on Figure 15. This shows reliabilities very near optimum from 10% to 60%. However, from 60% up to 100% the results seem to be very convoluted. As before, plotting a cumulative distribution graph shows that the reliability's behavior from 60% to 100% is due to poor sampling at those levels. Figure 16 illustrates this very clearly. The percentage of forecasted POSH data contained between 10% and 60% is 97%. Therefore, due to low sampling of POSH values greater than 60%, it is impossible to gather any reasonable interpretation from the POSH reliability results over these values. However, Tables 11 and 12 show that when the

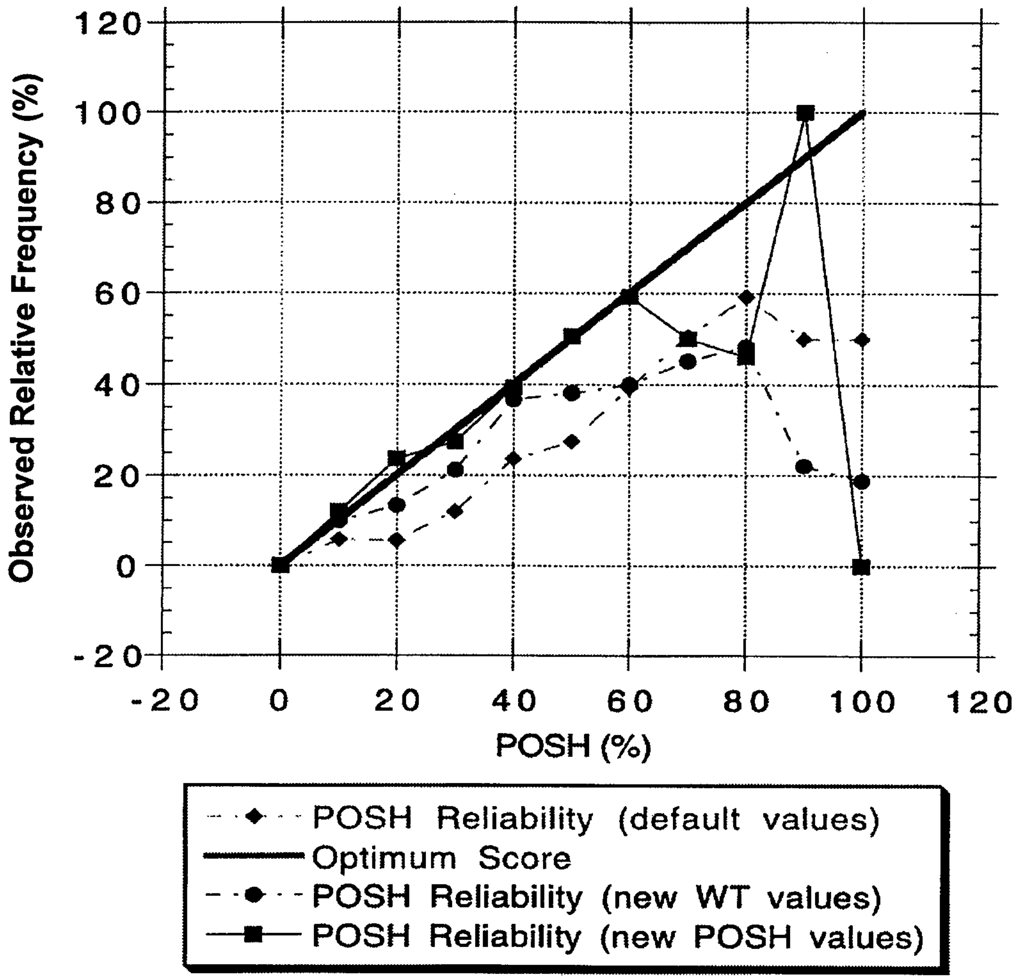

Figure 15. Same as Figure 13, except this figure includes the results from altering the POSH probability equation.

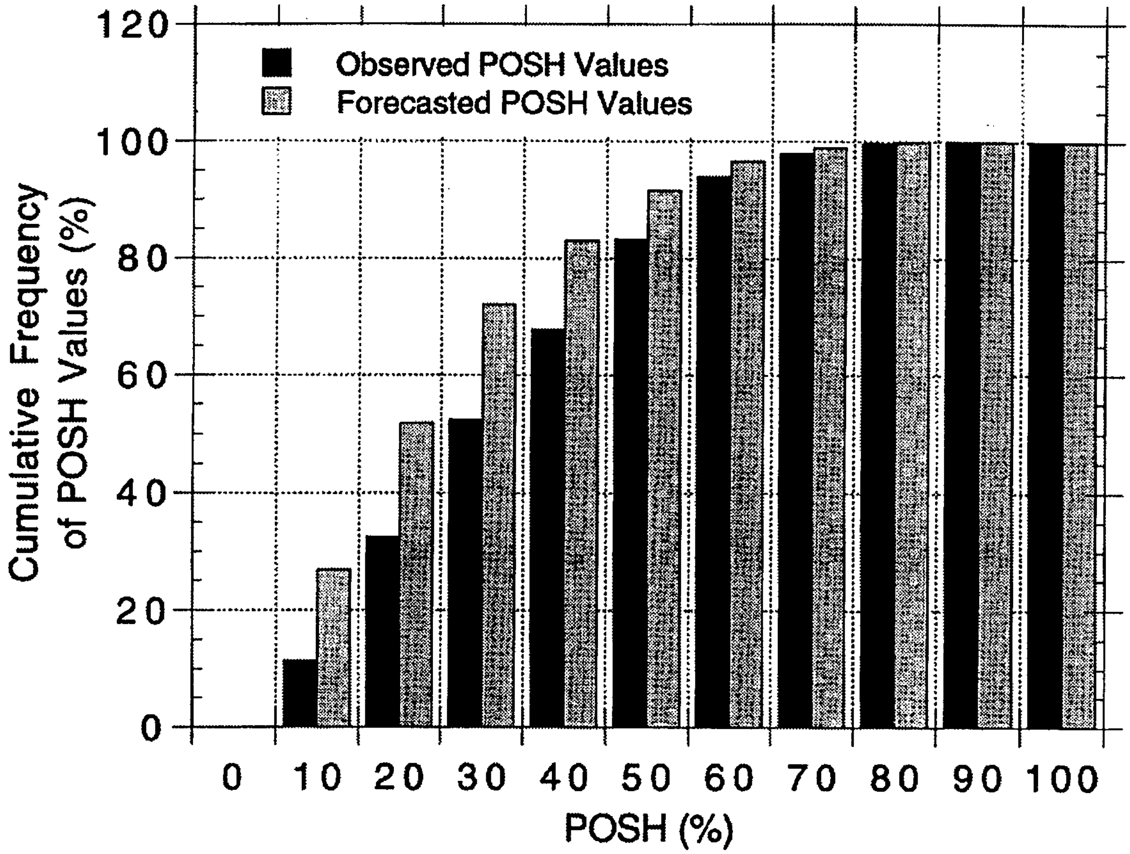

Figure 16. Same as Figure 10, except this figure shows the statistical results from running the hail algorithm after altering the POSH probability equation.

Table 11. Same as Table 9, except this table shows the statistical results from running the hail algorithm using an optimized POSH equation.

Seabreeze Data								
Date	**H_0 (km)**	**WT**	**H**	**M**	**FA**	**POD**	**FAR**	**CSI**
3 Jun 96	4.50	138	7	1	3	88	30	64
2 Jun 96	4.29	126	4	4	0	50	0	50
4 Jun 96	4.14	117	3	17	7	15	70	11
21 May 97	4.35	129	4	0	1	100	20	80
2 Sep 97	4.30	126	1	1	1	50	50	33
Average from Seabreeze Events						**45.24**	**38.71**	**35.19**

Continental Data								
Date	**H_0 (km)**	**WT**	**H**	**M**	**FA**	**POD**	**FAR**	**CSI**
21 Jan 98	3.98	108	13	9	13	59	50	37
22 Jan 98	3.96	107	19	25	11	43	37	35
9 Sep 97	4.60	144	11	12	13	48	54	31
3 Nov 95	4.15	118	7	16	12	30	63	20
25 Apr 97	3.72	93	6	10	4	38	40	30
11 Apr 97	3.70	92	7	23	4	23	36	21
28 May 97	4.10	115	4	4	1	50	20	44
2 May 94	3.96	107	19	1	8	95	30	68
5 Apr 94	4.23	122	10	7	7	59	41	42
15 Apr 94	4.08	114	13	16	36	45	74	20
11 May 95	4.53	140	8	19	23	30	74	16
27 Apr 97	4.42	133	2	23	4	8	67	7
5 Apr 96	3.80	98	25	8	34	76	58	37
Average from Continental Events						**45.43**	**54.14**	**29.75**
Overall Average from League City Study						**45.40**	**52.75**	**30.13**

Table 12. Same as Table 10, except this table shows the statistical results from running the hail algorithm using an optimized POSH equation.

Spring/Summer Data								
Date	**H_0 (km)**	**WT**	**H**	**M**	**FA**	**POD**	**FAR**	**CSI**
3 Jun 96	4.50	138	7	1	3	88	30	64
2 Jun 96	4.29	126	4	4	0	50	0	50
4 Jun 96	4.14	117	3	17	7	15	70	11
21 May 97	4.35	129	4	0	1	100	20	80
25 Apr 97	3.72	93	6	10	4	38	40	30
11 Apr 97	3.70	92	7	23	4	23	36	21
28 May 97	4.10	115	4	4	1	50	20	44
2 May 94	3.96	107	19	1	8	95	30	68
5 Apr 94	4.23	122	10	7	7	59	41	42
15 Apr 94	4.08	114	13	16	36	45	74	20
11 May 95	4.53	140	8	19	23	30	74	16
27 Apr 97	4.42	133	2	23	4	8	67	7
5 Apr 96	3.80	98	25	8	34	76	58	37
Average from Spring/Summer Events						**45.71**	**54.10**	**29.71**

Fall/Winter Data								
Date	**H_0 (km)**	**WT**	**H**	**M**	**FA**	**POD**	**FAR**	**CSI**
2 Sep 97	4.30	126	1	1	1	50	50	33
21 Jan 98	3.98	108	13	9	13	59	50	37
22 Jan 98	3.96	107	19	25	11	43	37	35
9 Sep 97	4.60	144	11	12	13	48	54	31
3 Nov 95	4.15	118	7	16	12	30	63	20
Average from Fall/Winter Events						**44.74**	**49.50**	**31.10**

scoring algorithm was run with the new POSH output, it produced similar statistical results as the ones from the new WTSM.

6) RADAR CALIBRATION SENSITIVITY RESULTS

All reflectivities from a chosen subset of the data were increased by 2 dBZ and ran again through the scoring algorithm. Performance statistics were computed (shown on Table 13), as well as the reliability of the POSH algorithm (shown on Figure 17).

When compared with the statistics from the default algorithm run, the POD values looked very similar. However, in the dBZ-adjusted run the FAR values were close to 14% higher than the default values. This resulted in the dBZ-adjusted run having an approximate 10% decrease in CSI when compared with the default run. The reliability graph shows the dBZ-adjusted values with more optimal reliability values from POSH = 10%-30%. However, with the exception of POSH = 60%, the adjusted values become less reliable than the default run after POSH = 40%.

Looking at the distribution of forecasted POSH values between the default run and the dBZ-adjusted run illustrates the same results (Figure 18). In the lower values of POSH, the dBZ-adjusted POSH values are lower than the default values. This would account for the higher reliability values in Figure 17. However, as POSH increases the dBZ-adjusted values become greater than the default values. This shows that in the dBZ-adjusted run there is greater over-forecasting of the higher values of POSH.

Table 13. This table shows the statistical performance of the HDA when 2 dBZ were added to all reflectivity values. The total default values listed below come only from the 5 days tested.

Date	**POD (%)**	**FAR (%)**	**CSI (%)**
15 Apr 94	38	76	17
03 Jun 96	88	30	64
04 Jun 96	10	60	09
25 Apr 97	56	67	26
21 Jan 98	67	63	32
22 Jan 98	49	55	31
Total Values	**45**	**67**	**26**
Total Default Values	**44**	**58**	**27**

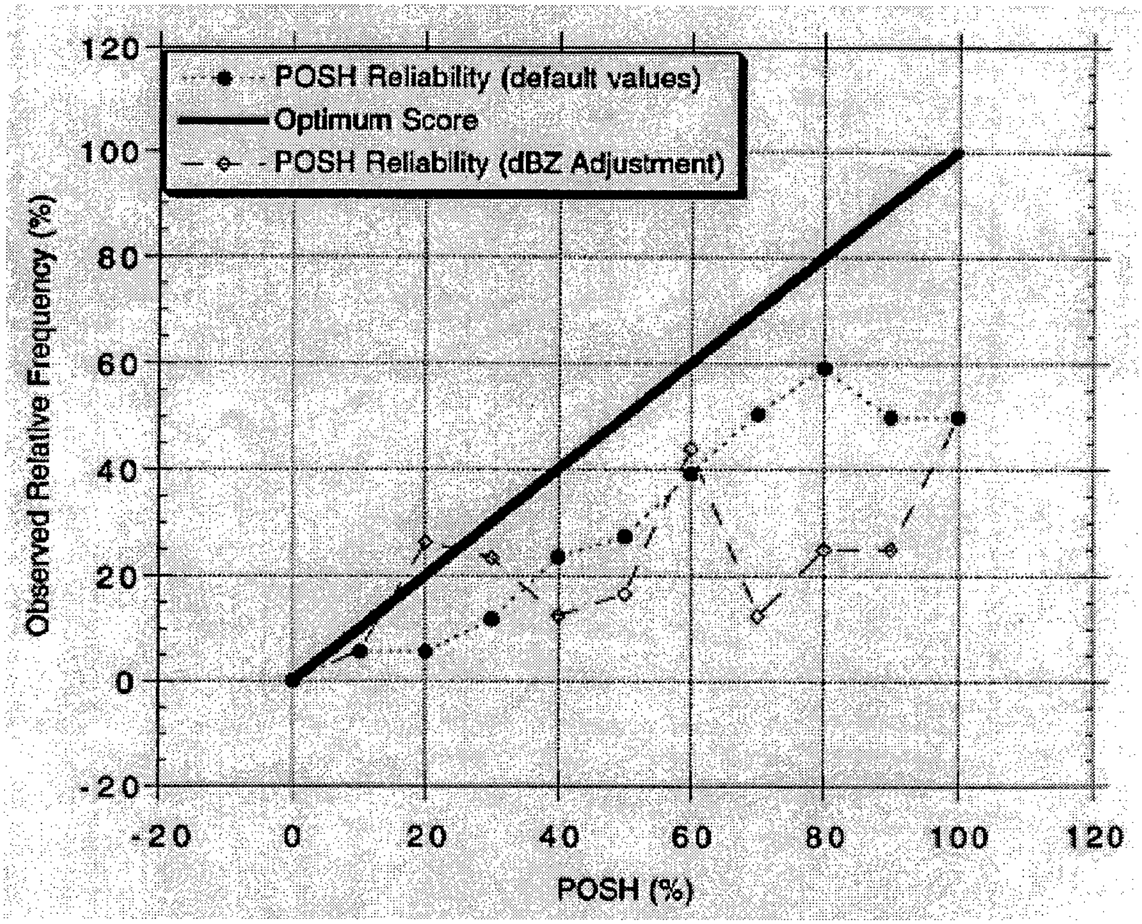

Figure 17. This figure shows the change in the reliability of a subset of data used to test the radar sensitivity to a 2 dBZ reflectivity adjustment. Default run values are shown by the circles. The POSH values of the dBZ-adjustment run are shown by the open diamonds.

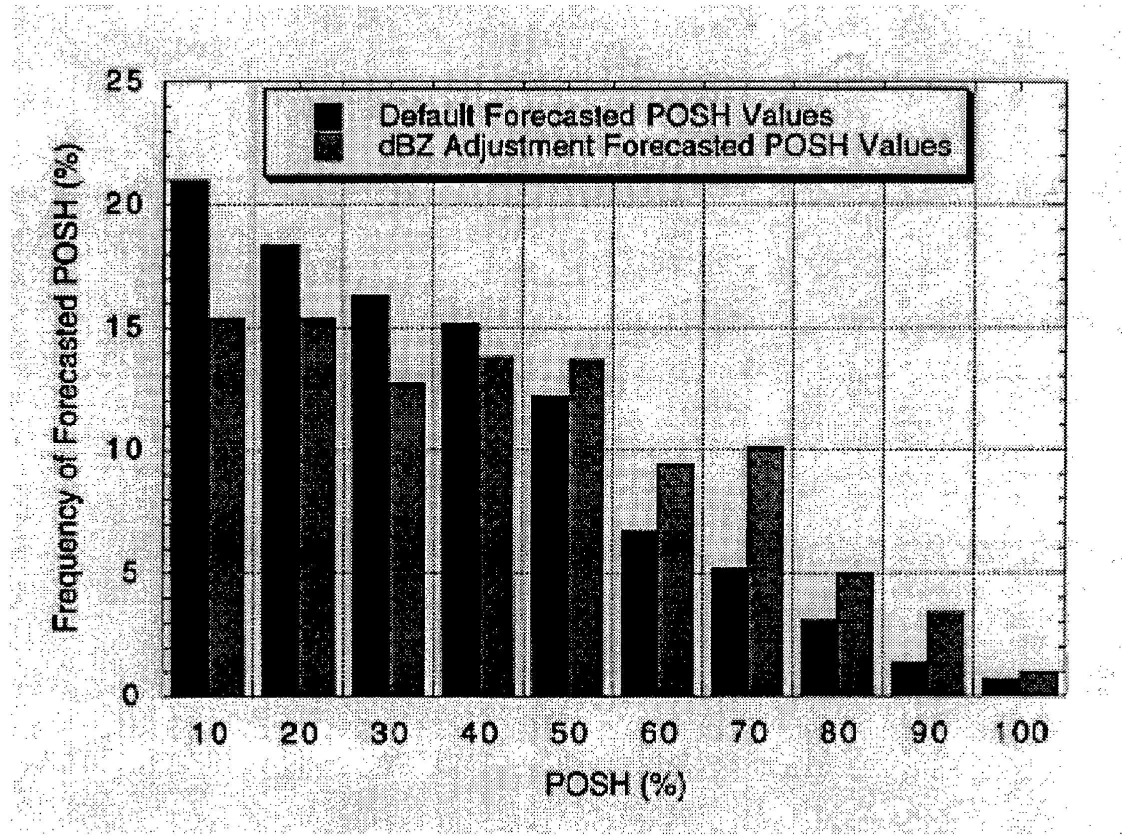

Figure 18. This figure shows the frequency of forecasted POSH values when the algorithm was run using the 2 dBZ adjustment. The default run values are shown in black, while the dbz-adjusted values are shown in gray.

CHAPTER V

CONCLUSIONS

The current version of WATADS contains several algorithms for detecting severe thunderstorms. They were built and installed in NWS offices with the intent that testing and optimization would be done by local offices. This becomes very important for empirically derived statistical algorithms that are tested in climates different from that for which they were developed. Unfortunately, these studies can become laborious and time-consuming for those examining the data. A simple method to optimize the hail algorithm over various regions of the U.S. would save NWS offices time and allow them to implement these changes in a quick and timely manner.

This study examined the performance of the NSSL hail algorithm for 18 different storm systems over the Gulf coast region in eastern Texas. This study ran the hail algorithm with all of the default values and then compared them with results from a NSSL regional hail study. It then presented adjustments to the POSH output of the current hail detection algorithm. These adjustments include optimizing the WTSM line, population density, and the POSH probability function. Using the default parameters, the hail detection algorithm over warned by about 20% over most of the range of values for the probability of severe hail.

When run with the default values, the algorithm's POD score for the League City area is lower than any region in the NSSL study. This would indicate that for this study there are a copious amount of algorithm misses for severe hail. However, this could be due to severe hail occurrences that failed to produce severe hail values for the entire 20-minute time-window. Still, both the FAR and CSI scores were comparable to the overall regional scores from the NSSL study. This could indicate initially that the hail algorithm runs optimally using the default values over the League City warning area.

Testing to see if the WT was correlated with the melting layer indicated the continental-Spring/Summer and the Spring/Summer data sets had good relationships between the optimal WT and the melting layer. The WTSM values chosen as optimal

were approximately two times larger than the default values. These values produced better statistical values than the default algorithm run, and could therefore be considered optimal for that data set, and possibly the region.

As well, optimizing the algorithm by changing the WTSM to provide the highest CSI for this data set improved the reliability of the POSH function for POSH values less than 60%. For reasons that may be related to the lack of sufficient observations for high POSH values, the performance of the optimized algorithm decreased relative to the default algorithm for POSH values greater than 60%.

Using a population density program to filter out hail data below a certain population threshold showed no improvement in the statistical scores. The highest overall POD, FAR, and CSI scores appeared when the population density thresholds were set at zero. This was predicted to occur when most of the hail data comes from rural areas (less than 100 persons per $4km^2$). This was shown to be true as the percentage of convective activity that occurred over the most populated region (1000 persons per $4km^2$) only included approximately 5% of what occurred over the entire data set. Therefore, it was not necessary to use any population density threshold for the data set of this study.

Since the over warning of the default algorithm was nearly constant, better reliability results were obtained by optimizing the algorithm directly through the POSH equation. The offset value of the POSH probability function was adjusted from +50 to +30. This alteration showed results very close to optimum on the reliability graph from POSH values 10% to 60%. Values greater than 60% showed reliability values worse than the default values. However, the POSH values greater than 60% accounted for only 3% of the entire data set. The lack of observations associated with high POSH values limits the proof of improvement in algorithm performance to POSH values less than 60%, and therefore, can be considered inconclusive. Statistical performance from the optimized POSH algorithm run showed results almost the same as the results from the optimized WTSM.

Two methods were used to optimize the POSH over the League City warning area. Optimizing the WTSM showed improvement of the statistical performance of the algorithm, but showed more ambiguous results with the reliability graph. Optimizing

the reliability of the POSH equation showed a more optimal graphical improvement, and showed the same statistical improvement to the HDA as did the newly optimized WTSM. This result is to be expected as multiplying the WT by a factor of two mathematically gives close to the same result as subtracting 20 from the POSH offset value (see Appendix B).

Even though optimizing both the WTSM and POSH showed improvements to the algorithm scores, it more importantly shows that a detailed WTSM study for a particular area may not be necessary, as optimizing the POSH equation through the reliability graph gives similar results. Simply optimizing the POSH equation could be a great time-saver as intensive warning threshold studies would require copious amounts of time in data-gathering and analysis. This could allow NWS offices to optimize their HDA more rapidly, thereby providing more accurate warnings to their area of responsibility.

The sensitivity to changes in the reflectivity values was also tested in this study. The results from the dBZ calculation error show that the performance of the HDA is susceptible to small variations in the interpretation of the reflectivity values by the radar. This finding has profound implications as it could lessen the validity of earlier hail algorithm studies if the radars used were not calibrated properly. Before any parameter adjustment to the hail algorithm is done, measures should be taken by each NWS office to ensure calibration is done to their radar.

With severe hail being a significant hazardous weather threat, it is important that a hail detection algorithm provide useful guidance to forecasters. The ability for weather software to include adjustable parameters in its algorithms greatly increases its usefulness to field operators. However, computer software is only as good as the hardware it runs on. To provide the most accurate adjustments to the hail algorithm software, the responsibility falls upon individual NWS offices to ensure their radar equipment is in proper working condition. The adjustments made to the POSH probability function in this study should improve the over-forecasting perception of the HDA, and hopefully lead to more accurate, effective hail forecasts over the Texas Gulf coast in the future.

REFERENCES

Battan, L. J., 1973: *Radar Observation of the Atmosphere*. Chicago, University of Chicago Press, 324 pp. [Reprinted by: Techbooks, Herndon, VA]

Browning, K. A., 1977: The structure and mechanisms of hailstorms. *Hail: A Review of Hail Science and Hail Suppression, Meteor. Monogr*., No. 38, Amer. Meteor. Soc., 1-43.

Changnon, S.A., 1968: Effect of sampling density on areal extent of damaging hail. *J. Appl. Meteor*., **7**, 518-521.

Crum, T.D., R. L. Alberty, and D. W. Burgess, 1993: Recording, archiving, and using WSR-88D data. *Bull. Amer. Meteor. Soc*., **74**, 645-653.

English, M., 1973: Alberta hailstorms. Part II: Growth of large hail in the storm. *Alberta Hailstorms, Meteor. Monogr.*, No. 36, Amer. Meteor. Soc., 37-98.

Federer, B., A. Waldvogel, W. Schmid, and H. H. Schiesser, 1986: Main results of Grossversuch IV. *J. Climate Appl. Meteor.*, **25**, 917-957.

Johnson, J. T., P. L. Mackeen, A. Witt, E. D. Mitchell, G. J. Stumpf, M. D. Eilts, and K. W. Thomas, 1998: The Storm Cell Identification and Tracking (SCIT) algorithm: An enhanced WSR-88D algorithm. *Wea. Forecasting*, **13**, 263-276.

Klazura, G.E., and D.A. Imy, 1993: A description of the initial set of analysis products available from the NEXRAD WSR-88d system. *Bull. Amer. Meteor. Soc.*, **74**, 1293-1311.

Lemon, L.R., 1978: On the use of storm structure for hail identification. Preprints, *18th Conf. On Radar Meteorology*, Atlanta, GA, Amer. Meteor. Soc., 203-206.

Miller, L. J., J. D. Tuttle, and C. A. Knight, 1988: Airflow and hail growth in a severe northern High Plains supercell. *J. Atmos. Sci.*, **45**, 736-762.

Nelson, S. P., 1983: The influence of storm flow structure on hail growth. *J. Atmos. Sci.*, **40**, 1965-1983.

NOAA, 1995: *Storm Data*. Vol. 37, No. 4-9. NESDIS, National Climatic Data Center, Asheville, NC.

______, 1996: *Storm Data.* Vol. 38, No. 3-10. NESDIS, National Climatic Data Center, Asheville, NC.

______, 1997: *Storm Data.* Vol. 39, No. 1-10. NESDIS, National Climatic Data Center, Asheville, NC.

Petrocchi, P.J., 1982: Automatic detection of hail by radar. AFGL-TR-82-0277. Environmental Research Paper 796, Air Force Geophysics Laboratory, Hanscom AFB, MA, 33 pp. [Available from Air Force Geophysics Laboratory, Hanscom AFB, MA.]

Smart, J.R., and R.L. Alberty, 1985: The NEXRAD Hail Algorithm applied to Colorado thunderstorms. Preprints, *14th Conf. On Severe Local Storms*, Indianapolis, IN, Amer. Meteor. Soc., 244-247.

Socioeconomic Data and Applications Center, 1995: Archive of Census Related Products. [Available electronically from www.ciesin.org]

Waldvogel, A., W. Schmid, and B. Federer, 1978a: The kinetic energy of hailfalls. Part 1: Hailstone spectra. *J. Appl. Meteor.*, **17**, 515-520.

_______, B. Federer, W. Schmid, and J. F. Mezeix, 1978b: The kinetic energy of hailfalls. Part II: Radar and hailpads. *J. Appl. Meteor.*, **17**, 1680-1693.

_______, _______, and P. Grimm, 1979: Criteria for the detection of hail cells. *J. Appl. Meteor.*, **18**, 1521-1525.

Wilks, D.S., 1995: *Statistical Methods in the Atmospheric Sciences*. Academic Press, 467 pp.

Winston, H. A., 1988: A comparison of three radar-based severe-storm-detection algorithms on Colorado High Plains thunderstorms. *Wea. Forecasting*, **3**, 131-140.

Witt, A., 1990: A hail aloft detection algorithm. Preprints, *16th Conf. On Severe Local Storms*, Kananaskis Park, Alta., Amer. Meteor. Soc., 232-235.

_____, 1993: Comparison of the performance of two hail detection algorithms using WSR-88D data. Preprints, *26th Intl. Conf. On Radar Meteorology*, Norman, OK, Amer. Meteor. Soc., 154-156.

_____, M.D. Eilts, G.J. Stumpf, J.T. Johnson, E.D. Mitchell, and K.W. Thomas, 1998: An enhanced hail detection algorithm for the WSR-88D. *Wea and Forecasting*, **13**, 286-303.

Wyatt, A., and A. Witt, 1997: The effect of population density on ground-truth verification of reports used to score a hail detection algorithm. Preprints, *28th Conf. On Radar Meteorology*, Austin, TX, Amer. Meteor. Soc., 368-369.

APPENDIX A
HAILSTORM INDICATORS

From the findings of Lemon (1978), several hail indicators were determined to be the most useful in representing the storm structure and the conditions necessary for hailstorm development (Smart and Alberty 1985). They are listed on Table A1. The hail algorithm used information from the Storm Centroid and Tracking Algorithms to test for the presence of these indicators (Smart and Alberty 1985). Figure A1 shows an illustration of a modeled hailstorm by the Storm Centroid Algorithm. After testing was completed, the storm was given one of the following four hail (of any size) labels: Positive, Probable, Negative or Unknown (insufficient data available to make a decision).

Table A1. Hail Indicators and their Assigned Weight Values. From Smart and Alberty (1985)

Indicators	Description	Assigned Weights
1	Highest detectable storm component ≥ 8km	17
2	Storm maximum reflectivity ≥ 55dBz	7
3	Mid-level storm component centroid > 1.0 km south of lowest component centroid	15
4	Mid-level storm component tilt is between 45° and 180° to the right of the storm direction	8
5	Mid-level storm component maximum reflectivity ≥ 50 dBz	20
6	Mid-level overhang ≥ 4km	15
7	Highest storm component exists above mid-level overhang	18
		Total : 100

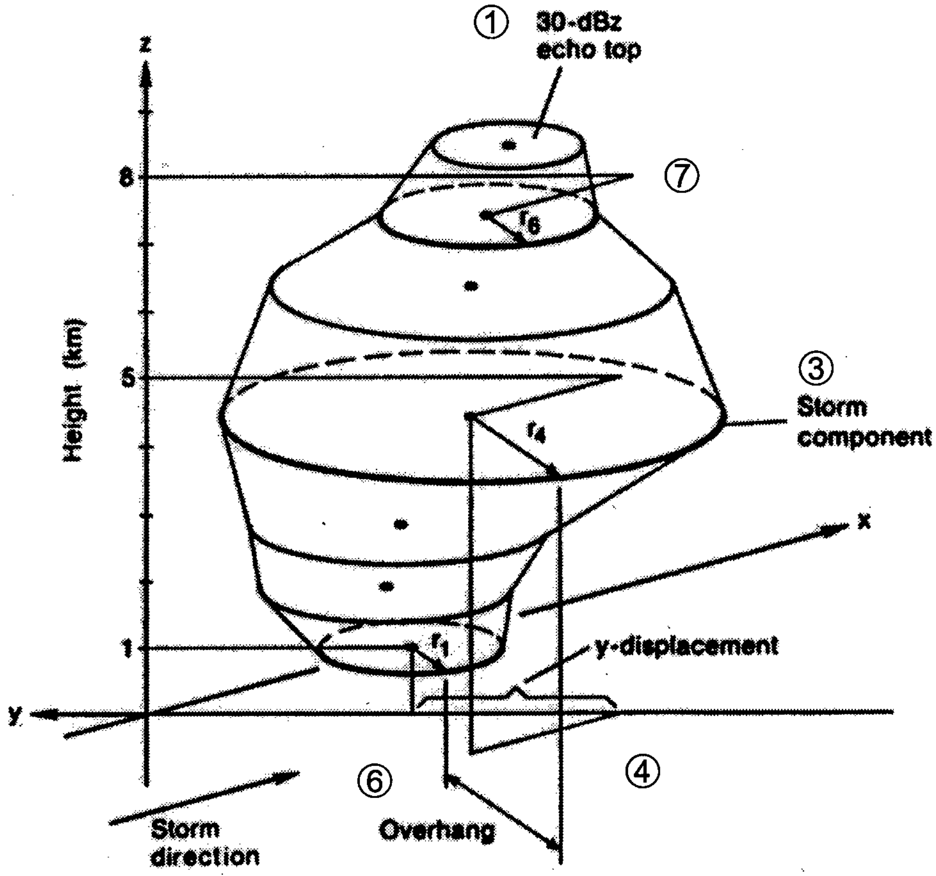

Figure A1. Illustration of a hailstorm as modeled by the NEXRAD storm identification algorithms. The numbers indicate five of the seven hail indicators listed on Table 1. Adapted from Smart and Alberty (1985).

APPENDIX B
DEFINITIONS OF RELAVENT ACRONYMS

CSI	Critical Success Index
dBZ	Logarithmic unit of (Z)
$\dot{E}$	Hailfall Kinetic Energy
FAR	False Alarm Rate
HCAA	Hail Core Aloft Algorithm
HDA	Hail Detection Algorithm
MEHS	Maximum Expected Hail Size
NCDC	National Climatic Data Center
NSSL	National Severe Storms Laboratory
NWS	National Weather Center
ORF	Observed Relative Frequency
POD	Probability of Detection
POH	Probability of Hail
POSH	Probability of Severe Hail
SCIT	Storm Cell Identification and Tracking Algorithm
SHI	Severe Hail Index
ULDA	Upper Level Divergence Algorithm
VIL	Vertically Integrated Liquid Water Content
WATADS	WSR-88D Algorithm Testing and Display System
WSR-88D	Weather Surveillance Radar-1988 Doppler
W(Z)	Reflectivity Weighting Function
WT	Warning Threshold
$W_T(H)$	Temperature-based Weighting Function
WTSM	Warning Threshold Selection Model

APPENDIX C
dBZ EXPLANATION

Simply put, dBZ is the logarithmic unit of the radar reflectivity factor (Z). The radar reflectivity factor is defined as the sum of the particle diameters raised to the sixth power per unit volume space sampled by the radar pulse (Battan 1973). Mathematically, Z is given by:

$$Z = \sum_{volume} D^6$$

where D is the diameter of the particle. The radar reflectivity factor is calculated for the return power measured by the radar receiver. These values can have a wide range depending upon the size of the particle observed by the radar. They can range from small particles, such as fog, which has a sample volume size of approximately 0.001 $mm^6\ m^{-3}$, all the way up to very large particles, such as hail, which can have a volume size of 36,000,000 $mm^6\ m^{-3}$ for softball-sized hail.

In order to account for these enormous variations in volume size, it is convenient to compress these values using a logarithmic scale. This leads to following equation, in which dBZ is the logarithmic reflectivity factor.

$$dBZ = 10\log_{10}\left(\frac{Z}{1mm^6 / m^3}\right)$$

APPENDIX D

$POSH'$ COMPUTATION

This computation will show that multiplying the WT by approximately 2 gives the same POSH results as decreasing the POSH offset by 20. Start with the original POSH equation:

$$POSH = 29\ln\left(\frac{SHI}{WT}\right) + 50$$

Now, multiply the WT parameter by 2 and separate the variables:

$$POSH = 29\ln SHI - 29\ln(2WT) + 50$$

Further separate the terms:

$$POSH = 29\ln SHI - 29\ln 2 - 29\ln WT + 50$$

Combining like terms gives:

$$POSH' = 29\ln\left(\frac{SHI}{WT}\right) + 50 - 20.1$$

or

$$POSH' = 29\ln\left(\frac{SHI}{WT}\right) + 29.9$$

This gives a $POSH'$ equation very similar to that of Eq. 7 in Chapter IV.